INVESTIGATION OF DYNAMIC NOISE AFFECTING GEODYNAMICS INFORMATION IN A TETHERED SUBSATELLITE

NASA GRANT NAG5-458

Semiannual Report No. 1

For the period 1 August 1984 through 31 January 1985

Principal Investigator

Dr. Gordon E. Gullahorn

January 1985

Prepared for
National Aeronautics and Space Administration
Greenbelt, Maryland 20771

Smithsonian Institution
Astrophysical Observatory
Cambridge, Massachusetts 02138

The Smithsonian Astrophysical Observatory
is a member of the
Harvard-Smithsonian Center for Astrophysics

The NASA Technical Officer for this Grant is Mr. Jean E. Welker, Code 921 Earth Survey Applications Division, Goddard Space Flight Center, Greenbelt, Maryland 20771.

INVESTIGATION OF DYNAMIC NOISE AFFECTING GEODYNAMICS INFORMATION IN A TETHERED SUBSATELLITE

NASA GRANT NAG5-458

Semiannual Report No. 1

For the period 1 August 1984 through 31 January 1985

Principal Investigator

Dr. Gordon E. Gullahorn

January 1985

Prepared for
National Aeronautics and Space Administration
Greenbelt, Maryland 20771

Smithsonian Institution
Astrophysical Observatory
Cambridge, Massachusetts 02138

The Smithsonian Astrophysical Observatory
is a member of the
Harvard-Smithsonian Center for Astrophysics

The NASA Technical Officer for this Grant is Mr. Jean E. Welker, Code 921 Earth Survey Applications Division, Goddard Space Flight Center, Greenbelt, Maryland 20771.

Introduction:

This Semiannual Status Report summarizes the work performed under Grant NAG5-458 entitled "Investigation of Dynamic Noise Affecting Geodynamics Instrumentation in a Tethered Subsatellite."

During the reporting period, SAO has

- Continued modeling of the atmospherically induced dynamic noise in the subsatellite through the modification and use of the SKYHOOK program.
- Written and submitted an invited paper for the forthcoming Special Issue on Geodynamics of the IEEE Transactions on Geoscience and Remote Sensing.
- Cooperated with Prof. Silvio Bergamaschi of the Institute of Applied Mechanics in Padova (Italy) in developing an analytic model of the continuum tether/shuttle/subsatellite system.
- Begun study of random vibration analysis for modeling the TSS under atmospheric perturbation.

Modeling of Atmospheric Effects:

The numerical modeling being done at SAO is with a modified version of the SKYHOOK program, which simulates the TSS as set of discrete masses and connecting (massless) tether segments. As described in the Final Report to the previous contract, NAG5-325, we have added facility for superimposing spatial fluctuations on the standard atmospheric density routine and outputting the resultant accelerations of the subsatellite, together with ambient densities at each mass, for later analysis. The acceleration components found to be most elucidating are those tangent to the tether at its attachment to the subsatellite and or-

thogonal. Expressed this way, the effects of tether longitudinal vibrations are separated from the direct effects of atmospheric drag variations. Restrictions are that the subsatellite is considered a point mass (attitude dynamics and aerodynamic effects are not yet included) and that computational effort limits the number of masses to about 10 for routine use, hence limiting the frequency response of the system. So far, all cases considered have been limited to a tether deployed in the orbital plane, though this restriction is not inherent in the program.

One simple, yet important, enhancement of SAO capabilities was the adaptation of graphics tools allowing informative and compact display of the acceleration and spectral outputs. Compare the figures in this report with the hand drawn Figure 7-1 or the printer plots in Appendix D of the NAG5-325 Final Report .

We resolved a subtle problem in the standard SKYHOOK atmospheric density routine which had been causing an occasional sharp jump in the orthogonal acceleration component. The difficulty arose from an interaction of two factors: First, to eliminate residual deployment effects we have been forced to make two SKYHOOK runs for each case considered, a "reference" run with no atmospheric perturbation and a run with the perturbation we wish to study. The resulting accelerations are differenced before plotting, computing spectra or other analysis. Second, the atmosphere routine used simple linear interpolation in a table, result-

ing in a $\rho(h)$ curve with only piecewise continuous derivative.

Because the two runs are different, the subsatellite will be at slightly different altitudes in each and thus subject to slightly different drag. If both subsatellites are in the same tabular interval, this difference will be constant or vary only very slowly, causing minimal effect. But when one subsatellite crosses a tabular altitude, and thus is subject to a different density as function of altitude, this difference in drag takes a sharp jump.

To remedy this problem, we created a smoother atmospheric density routine. We first attempted to simply interpolate $\log(\rho)$, but ended up fitting a moderate order polynomial to the $\log(\rho)$ data (with independant variable $\sqrt{\text{altitude-100km}}$) at each tabulated temperature and interpolating in temperature. This produced the desired smoothness with no noticeable deterioration in execution time. Our scheme of differencing the two runs may still have some effect at very low frequencies, as the relative altitudes of the subsatellites change gradually over the run.

Tracking down this effect of altitude on drag did point up one interesting mechanism:

> Any variation in the subsatellites altitude due to tangent accelerations produced by the tether (approximately vertical) will cause a variation in the ambient atmospheric density, hence the drag experienced, hence the orthogonal (approximately horizontal) acceleration.

The version of SKYHOOK created during the previous contract had allowed only a single density perturbation, with a sharp cutoff between the enhanced (or diminished) region and unperturbed density; the region is elliptical in cross section and extends indefinitely to either side of the orbital plane. Apart from the obvious restriction to a single perturbed region, the sharp boundary results in very long integration time due to the peculiarities of the Gear integrator used to solve the differential equations of motion.

In the reporting period we have extended the allowed perturbations to include up to two hundred (possibly overlapping) regions each with a smooth cutoff to enhance computational efficiency. The parameters of each region are: a vertical radius, r_v; a horizontal radius, r_h; altitude of center, h_c; a distance "along orbit" from the start of the simulation, a_c; and an enhancement factor, e. Again, since we are concerned with deployment in or near the orbital plane, the density perturbations extend indefinitely perpendicular to the plane. First, we define a scaled radius

$$r = \sqrt{((h-h_c)/r_v)^2 + ((a-a_c)/r_h)^2}$$

where h is the altitude and a the "along orbit" distance. Then the density perturbation for a single region, relative to the "base" unperturbed density, is

$$\rho/\rho_{base} = 1 + e/(1+r^2)^2.$$

The region so defined has the same total mass (in a two dimensional sense) as the previous sharply bounded region with the same vertical and horizontal radii and enhancement factor. When there is more than one perturbed region, the right hand side of this equation is computed for each perturbation and they are all multiplied together to form the total perturbation.

We have analyzed four cases: smooth and sharp bounded regions; impinging on the subsatellite at 120 km and on the tether at 170 km altitude. All regions were circular with 20 km (effective) radius, and 20% enhancement.

A typical plot of the residual tangent and orthogonal accelerations experienced after encounter with the perturbation is given in Figure 1; the other cases were similar. Note the smoother nature, and much smaller magnitude, of the orthogonal acceleration.

The spectra of the accelerations produced in the various cases are also surprisingly similar. Figure 2 shows those for two cases: a smooth perturbation impacting directly on the subsatellite, and a sharply bounded perturbation impacting halfway up the tether. The sharp peaks corresponding to the spring-mass mode and the expected eight longitudinal vibration modes are clearly visible in the tangent acceleration. These unperturbed modes are mimicked

by the orthogonal acceleration, with the addition of a mode at very low frequency, possibly due to latitudinal vibration modes. The spectra are largely similar, though the peaks in the case with tether impact are smaller in magnitude; note that the background levels are the same in both cases. To compare in more detail we tabulated the frequencies and magnitudes of the spectral peaks from a printout. The frequencies are all very close, to within ±0.001 Hz. The magnitudes are plotted in Figure 3. The disturbances with smooth and sharp cutoffs, at subsatellite altitude, are very similar in both magnitude and relative strengths of the peaks. The disturbance at mid-tether altitude also excites the modes in roughly the same ratios, although with substantially less magnitude.

From Gross, Reber and Huang (1984) and Gross and Huang (1984), we know that the power spectral density of variations at 250 km is roughly a power law with exponent -3 at low spatial frequencies and -3 to -4 at higher frequencies. We have investigated how to create a set of perturbed regions for use by the current version of SKYHOOK which will have the same spectrum (as seen by the subsatellite traversing the atmosphere). This investigation is largely complete and will be detailed in the final report, but we have not yet developed a carefully tailored model atmosphere. To make full use of the theory we may wish to make some modifications to SKYHOOK (e.g., sum the perturbations rather than multiply them; use gaussian perturbations), but the

approximations used may not be any cruder than our knowledge of the actual atmosphere.

We have, however, created a set of 200 regions, with random centers (altitudes 120 to 220 km, random distance along track), random radii (up to 30 km vertical, 50 km horizontal) and random enhancement factors (in the range -0.5 to +0.5); all distributions being uniform. The induced accelerations are shown in Figure 4, and the spectra in Figure 5. The tangent acceleration is roughly similar to that produced by single regions, and in the spectrum we see the same peaks as before although more weakly (note the higher baseline). The same modes are being excited, but with more "noise" generated by the random forcing function. The orthogonal acceleration, however, is totally dominated by the direct effect of the drag variations, and its spectrum is featureless. For reference, the ambient density at the subsatellite is shown in Figure 6, along with its spectrum. These are similar in character to the orthogonal acceleration, as expected if we are seeing largely direct drag effects in the latter.

The above, with the exception of completing the work on generating a model atmosphere giving the power law spectrum, represents the anticipated simulation development during the present contract, except as specific questions may arise in attacking the problems of noise isolation and instrument interface. Directions in the future might include:

- Use of Maximum Entropy Method for spectral analysis.

Both theory and the experience shown in our figures indicate that we should expect a number of sharp peaks on a smoother background. This sort of spectrum is ideally suited to MEM techniques, which effectively use rational function approximations to the spectrum rather than the simple polynomial approximation of Fourier analysis, and are thus better able to represent sharp peaks or lines.

- Include subsatellite attitude dynamics and aerodynmics. As discussed in the attached paper (see the next section), rotational effects, particularly rotational acceleration, are very important for measuring gravity gradients. We do not currently include them in the SKYHOOK program.

- Add a damped wave (or set of such) to the perturbation options. This feature is suggested by observations of Gross and Huang (1984) and would also allow us to naturally include high spatial frequencies in the atmospheric model.

- Simplify the analysis tools; generate equilibrium initial conditions to avoid the current differencing with a reference simulation.

Paper Written for IEEE Transactions on Geoscience and Remote Sensing:

A paper entitled "Gravity Gradiometry from the Tethered Satellite System", by G. E. Gullahorn, F. Fuligni and M. D. Grossi, was written and submitted for the Special Issue on Geodynamics. This paper is largely of a tutorial or review nature, since our survey of the open (published) literature showed virtually nothing available, especially at an introductory level. The paper also provides a summary of some SAO efforts in the field.

The paper has been accepted for publication and a revised version is being prepared. A copy of the draft version is included as Appendix A of this report.

Cooperation with Prof. S. Bergamaschi:

In December Prof. Silvio Bergamaschi or the Institute of Applied Mechanics in Padova, Italy visited SAO. Though NAG5-458 provided no direct funds for his visit, we did spend several days discussing tether dynamics, particularly dynamic noise, with Prof. Bergamaschi. Prof. Bergamaschi is developing a model of the TSS in which the tether is a full continuum, and applying modal analysis to this model. We assisted him with some numerical mode calculations, and discussed some non-intuitive physical implications of the results. We hope to continue the cooperation in developing this model, which will provide both a valuable check on SKYHOOK numerical computations, and results not obtainable with SKYHOOK.

Random Vibration Analysis:

We have done some literature search and reading with an eye to finding methods applicable to the TSS. This study and analysis is still in an early stage.

References

S. H. Gross, C. A. Reber and F. T. Huang, "Large-Scale Waves in the Thermosphere observed by the AE-C Satellite," IEEE Trans. Geosci. Remote Sensing, vol. GE-22, pp. 340-352,1984.

S. H. Gross and F. T. Huang, "Medium Scale Gravity Waves in the Thermosphere Observed by the AE-C Satellite," preprint, 1984.

Figure Captions

Fig. 1. Accelerations, in gals, produced by a single atmospheric density enhancement impacting the subsatellite. Smoothly cutoff region, 20 km radius, 20% enhancement. Acceleration as a function of time is plotted, the component tangent to the tether on top and orthogonal on bottom. Impact with the enhanced region occurred before the data plotted, although some of the final direct effect is visible in the orthogonal component.

Fig. 2. Logarithm of the acceleration spectral magnitude plotted as a function of frequency (Hz). In each plot, the top spectrum is for the tangent component, the bottom for the orthogonal. The top plot is for the case illustrated in Figure 1, a single smoothly falling off enhancement impacting directly on the subsatellite. The bottom plot is for an equivalent region impacting on the tether at its center, sharply cut-off to avoid any direct impact on the subsatellite.

Fig. 3. Comparison of the magnitudes of spectral peaks. The peak magnitudes are on logarithmic scales. The top graph compares equivalent regions with sharp and smooth cutoffs, both impacting directly on the subsatellite. The bottom compares identical enhancements impacting on the subsatellite at 120 km altitude and on the tether only at 170 km altitude. In each graph, the top pair of lines is for the tangent component, the bottom for the orthogonal component.

Fig. 4. Accelerations produced by a model atmosphere with 200 randomly scattered enhancement regions. The orthogonal component (top graph) appears to be responding directly to the ambient atmospheric perturbation, while the tangent component (bottom graph) is more similar to the results from a single region model (Fig. 1).

Fig. 5. Spectra of the time series in Figure 4. Note that the tangent component spectrum shows distinct peaks corresponding to excited vibration modes, while the orthogonal component spectrum is largely featureless.

Fig. 6. The ambient atmospheric density experienced by the subsatellite in the simulation of Figures 4 and 5, and its spectrum. Note the similarity to the orthogonal component's graphs in Figures 4 and 5.

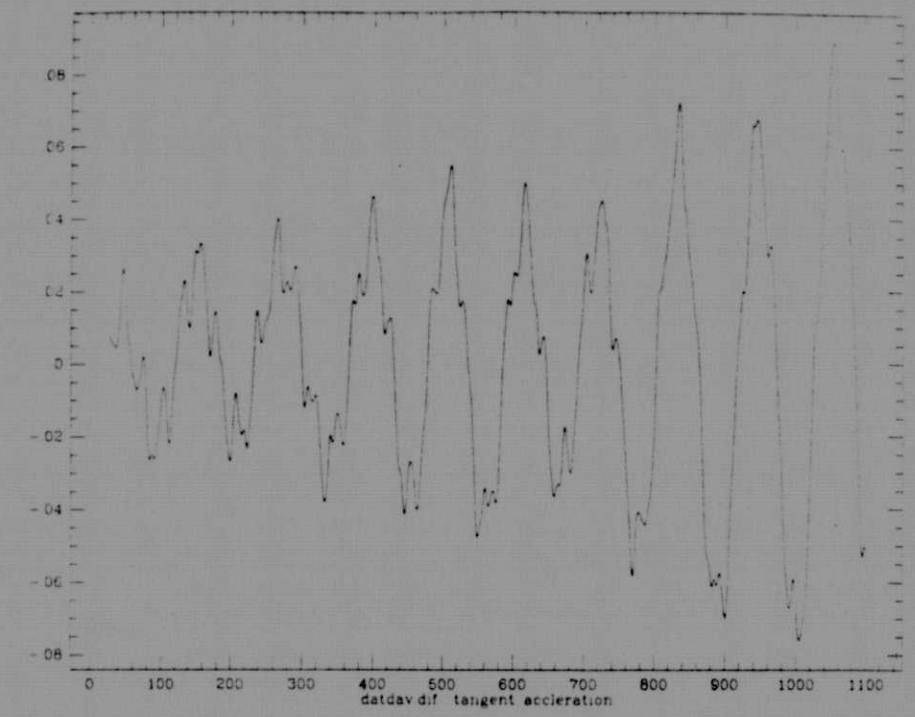
.08
.06
.04
.02
0
-.02
-.04
-.06
-.08
0
100
200
300
400
500
600
700
800
900
1000
1100
datdav dif tangent accleration

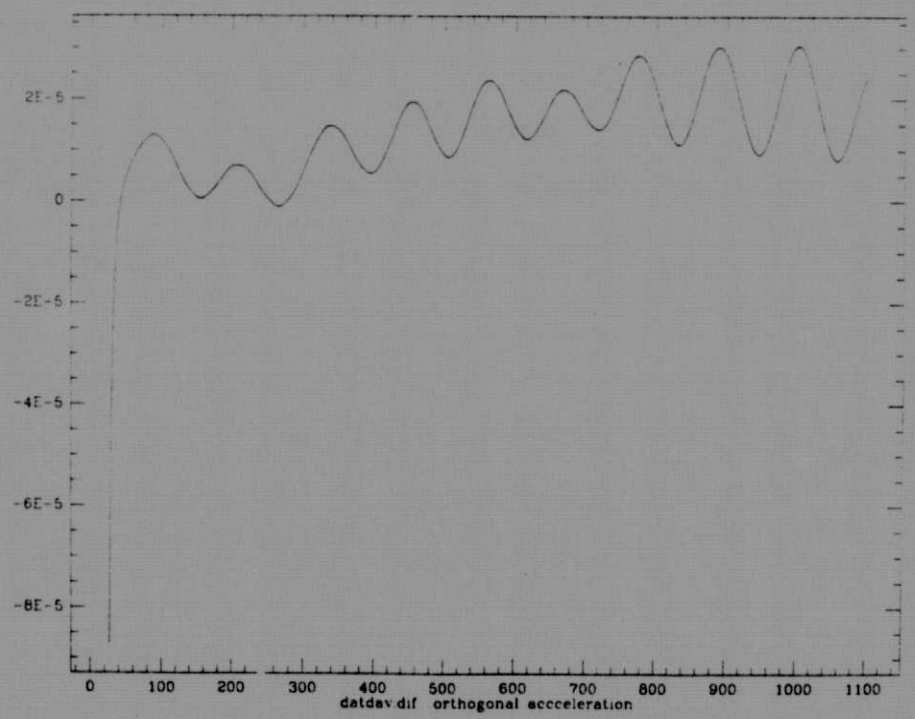
2E-5
0
-2E-5
-4E-5
-6E-5
-8E-5
0
100
200
300
400
500
600
700
800
900
1000
1100
datdav dif orthogonal accceleration

Figure 1

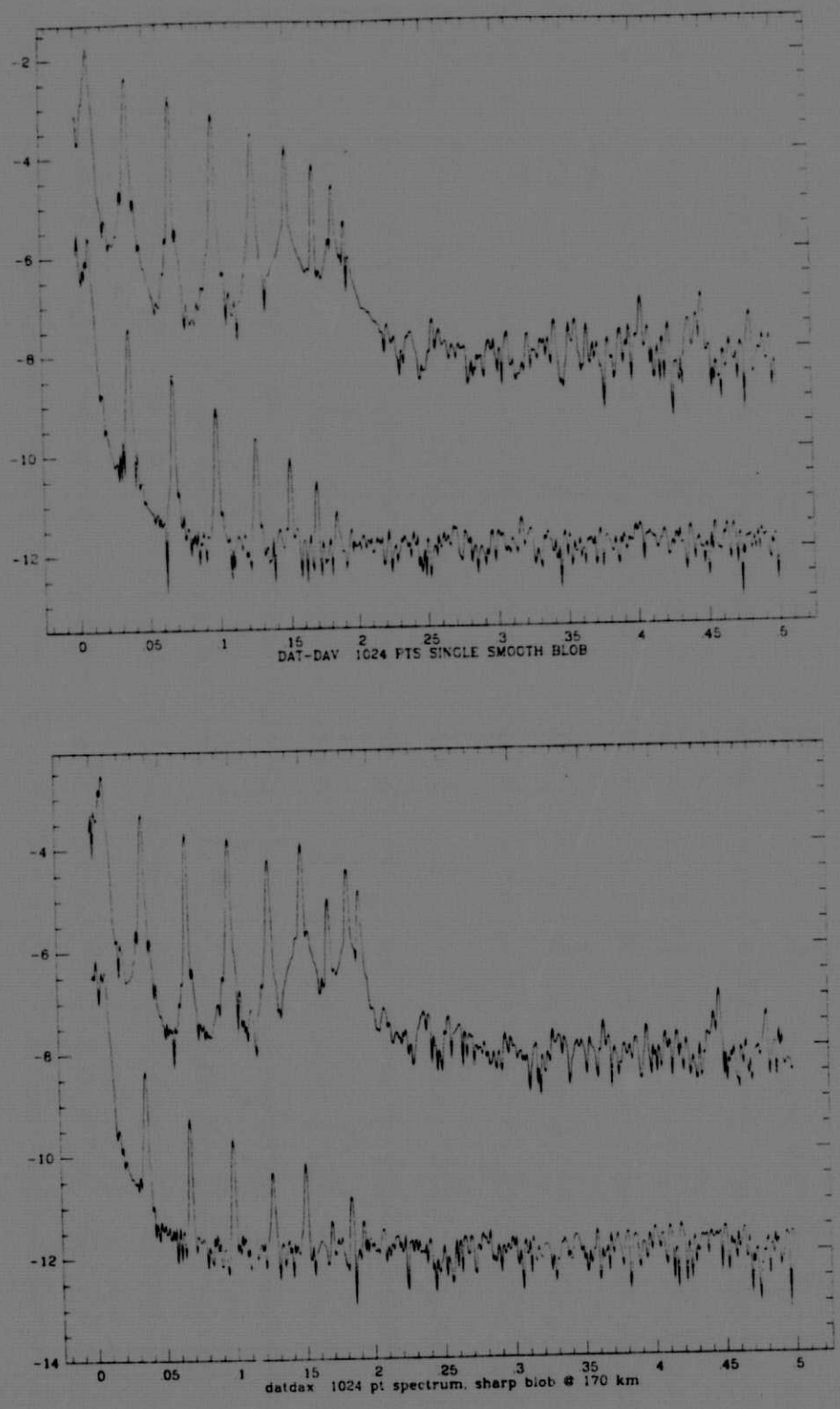
-2
-4
-6
-8
-10
-12
0
05
1
15
2
25
3
35
4
45
5
DAT-DAV 1024 PTS SINGLE SMOOTH BLOB
-4
-6
-8
-10
-12
-14
0
05
1
15
2
25
3
35
4
45
5
datdax 1024 pt spectrum, sharp blob @ 170 km

Figure 2

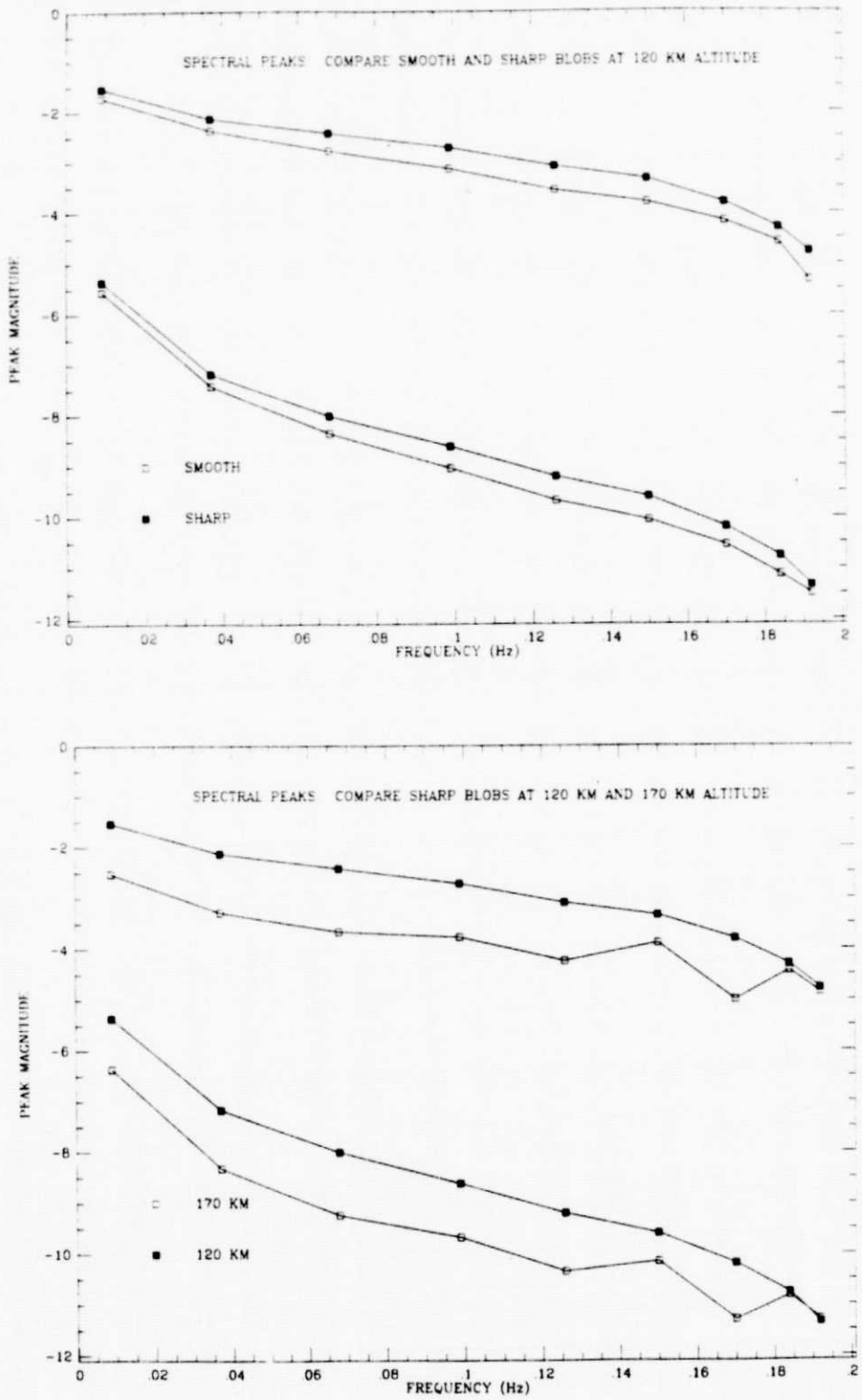
SPECTRAL PEAKS COMPARE SMOOTH AND SHARP BLOBS AT 120 KM ALTITUDE
PEAK MAGNITUDE
SMOOTH
SHARP
FREQUENCY (Hz)
SPECTRAL PEAKS COMPARE SHARP BLOBS AT 120 KM AND 170 KM ALTITUDE
PEAK MAGNITUDE
170 KM
120 KM
FREQUENCY (Hz)

Figure 3

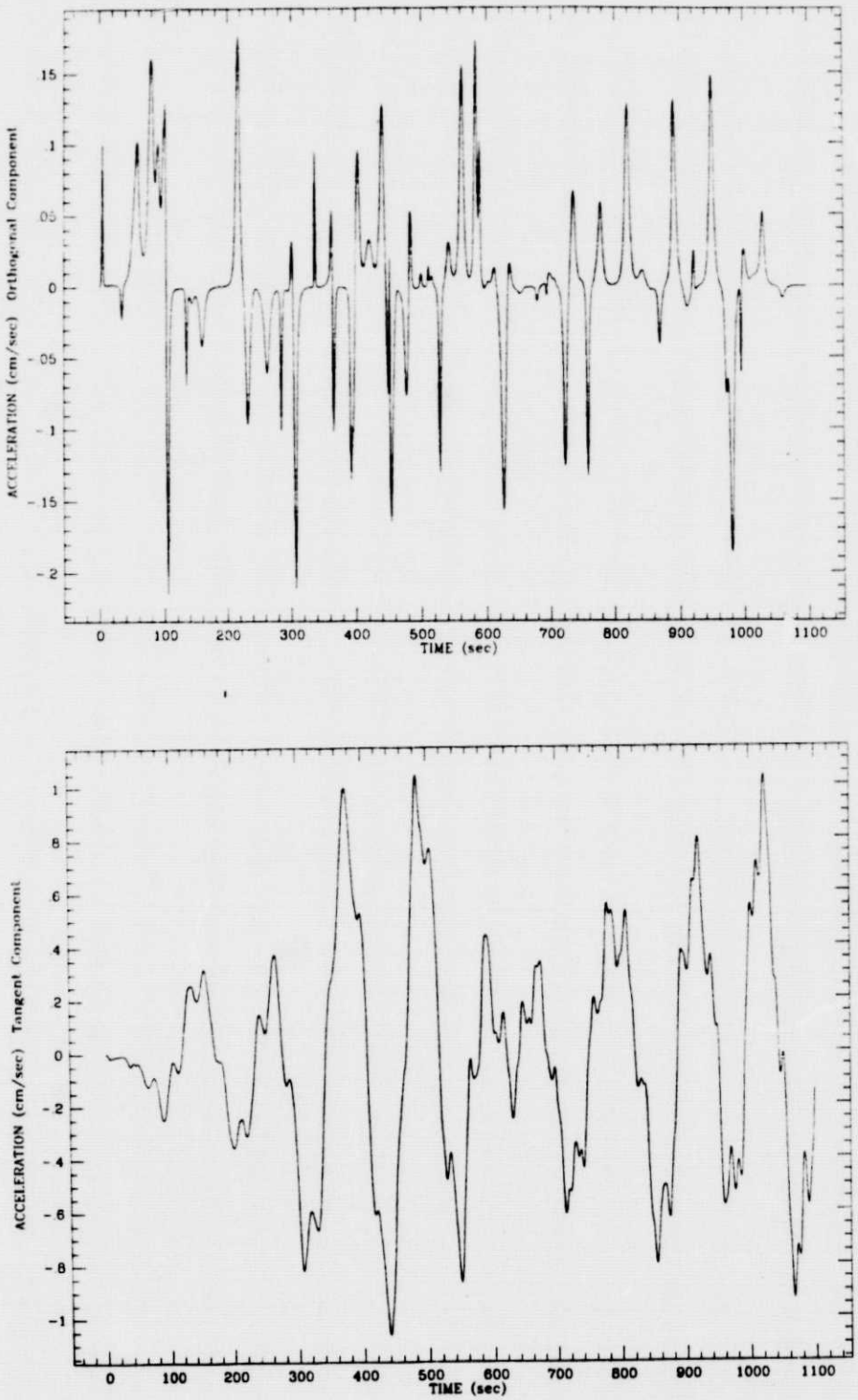
ACCELERATION (cm/sec) Orthogonal Component
15
1
05
0
-05
-1
-15
-2
0
100
200
300
400
500
600
700
800
900
1000
1100
TIME (sec)
ACCELERATION (cm/sec) Tangent Component
1
8
6
4
2
0
-2
-4
-6
-8
-1
0
100
200
300
400
500
600
700
800
900
1000
1100
TIME (sec)

Figure 4

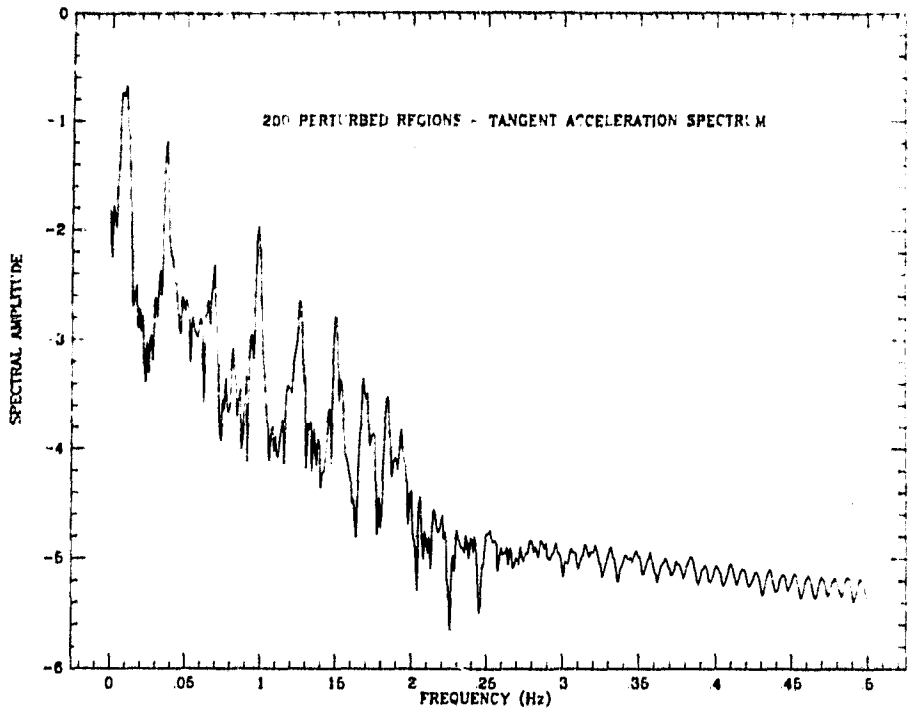
200 PERTURBED REGIONS - TANGENT ACCELERATION SPECTRUM
SPECTRAL AMPLITUDE
0
-1
-2
-3
-4
-5
-6
0
.05
1
15
2
25
3
35
4
45
5
FREQUENCY (Hz)

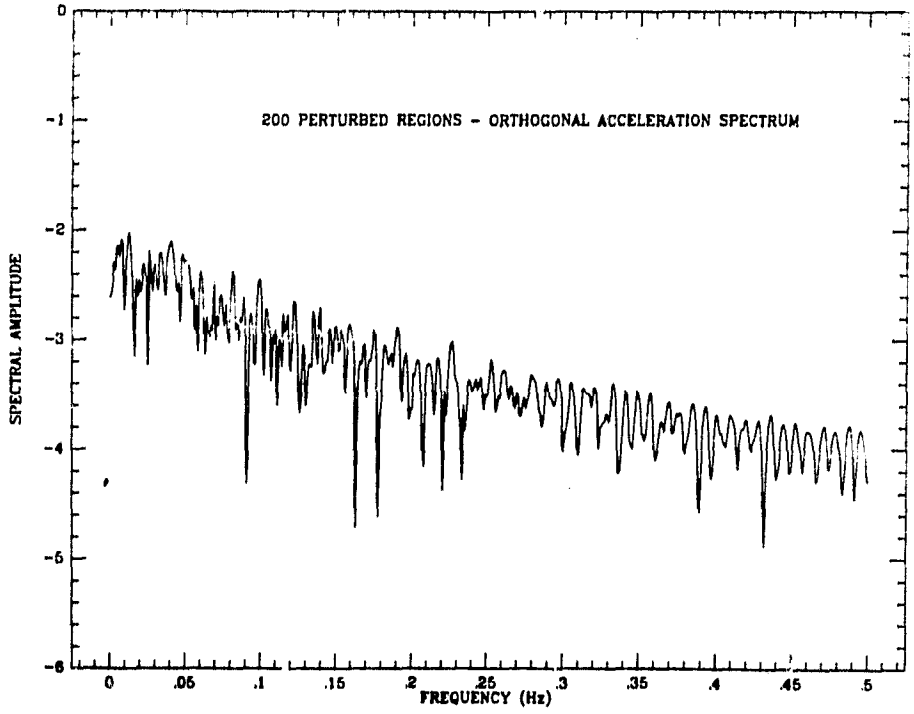
200 PERTURBED REGIONS - ORTHOGONAL ACCELERATION SPECTRUM
SPECTRAL AMPLITUDE
0
-1
-2
-3
-4
-5
-6
0
.05
.1
.15
.2
.25
.3
.35
.4
.45
.5
FREQUENCY (Hz)

Figure 5

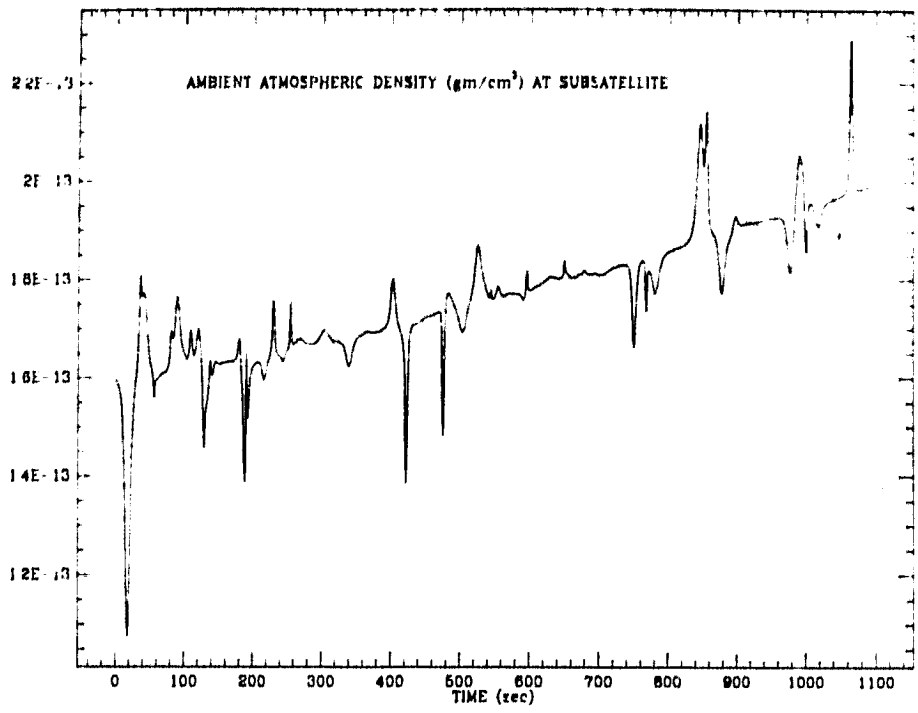
AMBIENT ATMOSPHERIC DENSITY (gm/cm³) AT SUBSATELLITE
1.8E-13
1.6E-13
1.4E-13
0
100
200
300
400
500
600
700
800
900
1000
1100
TIME (sec)

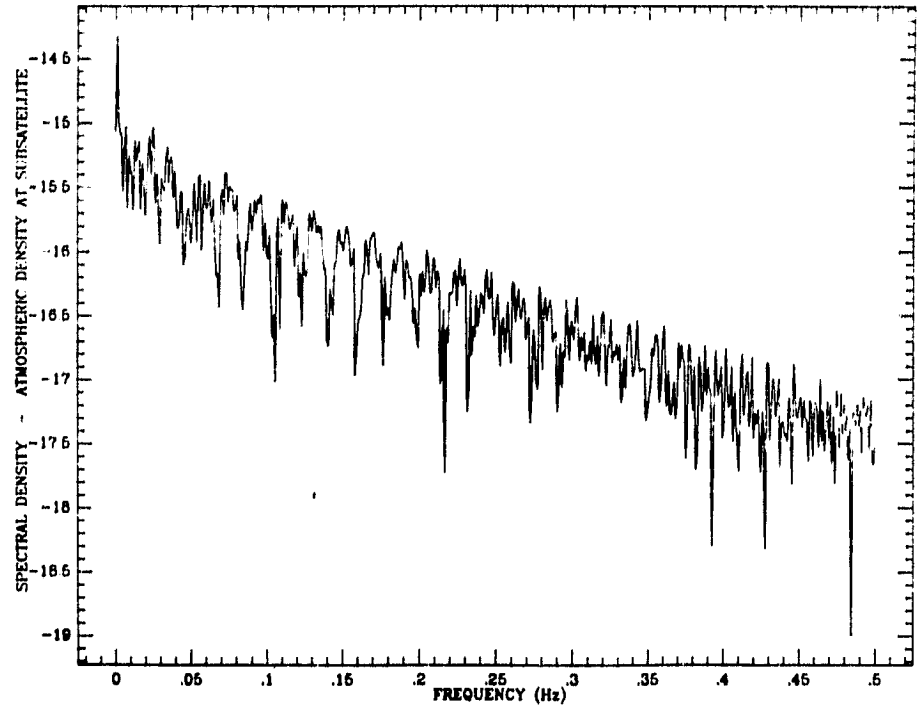
SPECTRAL DENSITY - ATMOSPHERIC DENSITY AT SUBSATELLITE
-14.5
-15
-15.5
-16
-16.5
-17
-17.5
-18
-18.5
-19
0
.05
.1
.15
.2
.25
.3
.35
.4
.45
.5
FREQUENCY (Hz)

Figure 6

A P P E N D I X A

Paper submitted to

IEE Transactions on Geoscience

and Remote Sensing

D R A F T C O P Y
****

Gravity Gradiometry from the Tethered Satellite System

by

Gordon E. Gullahorn

Franco Fuligni

Mario D. Grossi

Harvard-Smithsonian Center for Astrophysics

Submitted to IEEE Transactions on Geoscience and Remote Sensing

This work was supported by NASA Grant NAG5-458

G. Gullahorn and M. Grossi are with the Harvard-Smithsonian Center for Astrophysics, 60 Garden Street, Cambridge, Massachusetts 02138

F. Fuligni is a SAO Visiting Scientist from IFSI-CNR, Frascati, Italy

ABSTRACT

Measurement of the gradient of the gravitational acceleration from a satellite platform is likely to provide the next improvement in knowledge of the Earth's gravity field after the upcoming Geopotential Research Mission. Observations from the subsatellite of a Tethered Satellite System (TSS) would increase sensitivity and resolution due to the low altitude possible. However, the TSS is a dynamically "noisy" system and would be perturbed by atmospheric drag fluctuations. The dynamic noise is being modeled in order to evaluate the feasibility of TSS gradiometry and to design methods of abating the error caused by this noise. The demonstration flights of the TSS will provide an opportunity to directly observe the dynamical environment and refine modeling techniques.

I. INTRODUCTION

The problem of determining the Earth's gravitational field has engaged both the cleverness and the tenacity of natural scientists since the seventeenth century. The experimental methods and mathematical formulations employed have often been in the front ranks of current research; while the collection and analysis of the data is perennially a monumental task. In this paper we shall outline a promising proposed technique for refining our knowledge of the gravity field: measuring the (tensor) gradient of the gravity vector with instruments suspended some one hundred kilometers beneath an orbiting Space Shuttle.

The advantages of the proposed approach lie on three levels: measurements from orbit will be relatively uniform and rapidly obtained, compared to surface based observations; gradiometric measurement, as opposed to gravity field reconstruction from orbital perturbations, emphasizes short scale anomalies; and operation from a tethered subsatellite, at a lower altitude than possible from a free flying satellite, increases both the overall sensitivity and the short scale response. The tethered satellite system (TSS), however, possesses many natural modes of vibration and will be subjected to perturbing forces, including fluctuations in atmospheric drag. Methods of abating the resulting dynamic noise, either by physical damping mechanisms or in data processing, will at the least provide a challenge to the experiment designers. The noisy environment may even outweigh the advantages of low altitude operation, making a free flying (possibly drag compensating as with GRM) satellite platform more attractive for gradiometric measurements.

It is our purpose here to place TSS gradiometry in context, and to provide a snapshot of current work toward assessing its feasibility.

II. THE GRAVITY FIELD AND ITS MEASUREMENT

A. The Gravity Field and Anomalies

A spherically symmetric Earth would have a spherically symmetric gravity field, the gravitational acceleration vector pointing toward the center, with magnitude GM/r^2 external to the body; G is the gravitational constant 6.67×10^{-8} dyn cm^2 g^{-2}, M the total mass, and r the distance from the center. The gravitational potential is simply $U = -GM/r$, and the acceleration is $\bar{g} = -\nabla U$. Deviation from spherical symmetry in the mass distribution leads to a non-symmetric potential, allowing us to obtain information about the internal distribution by observing the external gravitational field; although an observed field does not uniquely determine the mass distribution, combination with reasonable physical assumptions and other data provides valuable results. (For brief surveys of this geophysical material see [1], [2] and [3], and for more detail, [4] and [5].)

The gravitational field of a body is commonly expressed by expanding the potential in spherical harmonics:

$$U = (GM/r) \sum_{m=0}^{\infty} \sum_{n=0}^{m} (R/r)^m Y_{mn}(\phi,\lambda) \qquad (1)$$

where

$$Y_{mn} = P_{mn}(\sin\phi)\ [C_{mn}\cos n\lambda + S_{mn}\sin n\lambda\ ] \qquad (2)$$

Here P_{mn} is a Legendre function and R is the Earth's radius. Y_{mn} will have wavelength $2\pi/m$ in ϕ and $2\pi/n$ in λ, and thus to resolve a feature of size x in the potential field at the Earth's surface, one must retain terms through order $m = \pi R/x$ (where a half-wavelength criterion is used). For x = 100 km, this leads to m = 200; i.e., some 20,000 terms (40,000 coefficients C_{mn} and S_{mn}).

Although this formulation is convenient for much theoretical work and detailed modeling, and particularly appropriate when discussing the large scale features of the gravity field, for our purposes, focused on short scale effects and on intuitive feasibility arguments, the"flat Earth" approximation generally proves more informative. The Earth is considered as a horizontal plane, infinite in extent. The case corresponding to spherical symmetry is planar symmetry in the mass distribution; the gravity vector will then be directed vertically, with magnitude $g = -2\pi G\sigma$ (independent of height above the Earth) where σ is the surface density, that is, the total mass beneath a unit area. As in the spherical case, departure from perfect planar symmetry will also perturb the gravity field; however, one is typically concerned not with a global expansion such as (1), but more directly with the local anomalous distribution.

In either framework, a <u>gravity anomaly</u> is a departure of the gravity field from some smooth reference field; in the case of a full spherical treatment, this is typically a reference ellipsoid, while in the flat earth approximation, the reference could be a plane symmetric field corresponding to the mean surface density. Various corrections must be applied to the observed anomaly, e.g. to "sea level" or for the mass (of the local

topography such as mountain ranges) between the observation and sea level, and there are consequently various forms of the anomaly (see the references for details). These complications largely vanish for spacecraft observations, and we shall always mean an anomaly at sea level but uncorrected for local topography, the "free air" anomaly. The quantity generally discussed is the vertical component of the anomalous gravitational acceleration, and the appropriate unit is the milligal (1 mgal = 10^{-3} cm/sec^2). Typical large scale anomalies are tens of milligals. A one milligal anomaly corresponds to a surface density enhancement of 2.4 x 10^3 g/cm^2.

Anomalies are due to local topography such as mountains (which can be corrected for) and to variations in the subsurface density distribution; the latter effect is of primary interest. The scale of an anomaly is roughly the scale of the density variation; accurate observation of anomalies on scales around a hundred kilometers would allow exploration of a variety of phenomena of geophysical interest, such as subduction zones and mantle convection. NASA's Geopotential Research Program [6] has established as a long term objective an accuracy of 0.5-1 mgal at a resolution of 50 km, with interest in features down to 25 km (comparable to the thickness of the lithospheric crust).

B. Current Gravity Measurement Techniques

The historical methods of measuring the gravity field produce local data, at discrete points on or near the Earth's surface. The methods are extreme refinements of simple concepts, such as timing a pendulum's period, measuring the displacement of a spring balance, or observing the acceleration of a falling body. These methods can provide precise short

scale information, but are exacting to make, require correction for local topography, are only available for a portion of the Earth's surface, and widely separated measurements are difficult to calibrate.

A more recent addition to the arsenal is the observation of satellite orbits, initially with photographic methods but currently by laser ranging from ground stations and altimeter data over the oceans. The irregularities in the gravity field gradually perturb the orbit, allowing one to fit for the coefficients in the spherical harmonic expansion of the potential (1,2). The resulting models have opposite emphasis from the surface measurements, being most accurate at large scales. The most accurate current results are the Goddard Earth Models (GEM's), some of which also incorporate surface data. The accuracy of GEM10B, at a resolution of $1^{\circ} \times 1^{\circ}$, is about 20 mgal over continents and 8 mgal over oceans. (See the summary in [6].)

C. Geopotential Research Mission

An experiment to be flown in the early 1990's, the Geopotential Research Mission (GRM) [7], will provide a dramatic improvement in our knowledge of the Earth's gravity field. The mission will consist of two satellites in the same 160 km altitude orbit, separated by several hundred kilometers. The satellites will be effectively drag free: each will contain a test mass shielded from the atmosphere, and hence traveling in a purely gravitational orbit, together with sensors and thrusters so that the remainder of the satellite can imitate the orbit of the test mass. Their relative velocity will be very precisely measured by dual frequency Doppler tracking. Any irregularity in the gravitational field will produce non-zero relative velocities, so that one can fit for the coefficients in

the field expansion (1,2) from the velocity data. The expected accuracy is 1 mgal [7] or 2 mgal [6] at 100 km resolution (about 1^{o}).

D. Gravity Gradiometry

The traditional methods for point gravitational measurements described in Section B above all measure the gravitational acceleration and thus require a fixed platform (or one connected to the solid Earth through the hydrosphere or atmosphere). They cannot be applied from a platform in free fall, such as an orbiting satellite, despite the advantages of coverage and speed this would provide. However, it is also possible to measure the gradient of the gravity field, i.e. the variation of the acceleration vector over some small spatial interval, and this technique is applicable to satellite measurements. In contrast to the orbital perturbation method, gravity gradient measurements respond directly and immediately to anomalies as the satellite passes near them; one can also use the data to fit a model of the form (1), but for intuitive understanding and possibly also for data analysis [8] the direct influence is more enlightening. (Gradiometry has recently found application to surface measurements [9] [10], but we shall only consider satellite measurements.)

The gravity gradient is a tensor whose components in Cartesian coordinates are defined as

$$W_{ij} = \partial g_i/\partial x_j = - \partial^2 U/\partial x_i \partial x_j \qquad (3)$$

The gravity gradient is expressed in Eötvös units, 1 EU = 10^{-9} gal/cm = 10^{-9} sec^{-2}. Note that because the gravity vector arises from a potential, $W_{ij} = W_{ji}$; and in free space Poisson's equation will relate the three

diagonal components, $W_{xx} + W_{yy} + W_{zz} = 0$. Thus, of the nine components, only five are truly independent.

Measurements made with an instrument linearly accelerated relative to a rest frame will not be affected due to the phenomenon of common mode rejection discussed below. However, if the instrument is subject to a rotation with angular velocity $\bar{\omega}(t)$, the measured gradient will be

$$W^{meas} = W^{rest} + \dot{T} + T^2 \tag{4}$$

where W^{rest} is the gradient of (3), T(t) is the matrix

$$T(t) = \begin{bmatrix} 0 & -\omega_3 & \omega_2 \\ \omega_3 & 0 & -\omega_1 \\ -\omega_2 & \omega_1 & 0 \end{bmatrix} \tag{5}$$

and T^2 means matrix multiplication in the common sense. Note that the term dependent on the angular <u>acceleration</u> is anti-symmetric and can be immediately distinguished from the inertial frame gradient if the measurements are accurate enough; the term dependent on the angular <u>velocity</u> is symmetric, and cannot be removed from the observations without knowledge of the instruments rotation.

The gravity field is a linear functional of the mass density distribution. Thus, the gradient due to a point mass, the impulse function as it were, is of interest. In Cartesian coordinates, the gradient due to a point mass M at the origin is simply

$$W_{ij} = (GM/R^3)\ \{3(x_i/R)(x_j/R) - \delta_{ij}\} \tag{6}$$

where R is the distance from the origin and δ_{ij} is the Kronecker delta. To put this in a more useful format, let us return to the "flat Earth" scenario. Consider a satellite moving at constant altitude Z above the X-Y plane. We then have

$$W = (GM/Z^3)(1/r^5) \begin{bmatrix} 3x^2-r^2 & 3xy & 3x \\ 3xy & 3y^2-r^2 & 3y \\ 3x & 3y & 3-r^2 \end{bmatrix} \qquad (7)$$

where $x = X/Z$, $y = Y/Z$, $r = R/Z$. This format emphasizes two factors: a strength factor, GM/Z^3, depending only on the altitude Z; and a shape factor which depends only on the geometry, i.e. on the horizontal distances scaled by the altitude.

If the satellite moves parallel to the X axis then the gradient is a function of one along-path coordinate X; the set of shape functions is plotted for several values of the scaled offset y in Fig. 1. For a path directly over the anomaly ($y = 0$), the width of the response is about unity in the scaled coordinate x (indeed, for W_{zz}, FWHM = 1.0014), that is, the width is about the altitude; the values of those components which are not identically zero are of order unity also. As the offset becomes larger, the gradients become smaller and the width of the shape function increases, though the effect is not pronounced for offsets smaller than the altitude. For a satellite moving with constant velocity, these plots (appropriately relabelled) show instrument response as a function of time. At a velocity of 7.6 km/sec the temporal width of the impulse functions due to an anomaly immediately below the flight path will then be about 16 sec at 120 km altitude and 29 sec at 220 km.

The radial component of the gradient due to a point mass is seen to predominate (W_{zz} of (7) with $x = y = 0$). This is $W_{rr} = 2GM/r^3$. The gradient due to the full Earth mass at the surface is about 3000 EU. This unavoidable background imposes a substantial dynamic range requirement when compared to the signals due to anomalies: The goal for anomaly detection, a 50 km square 0.5 mgal anomaly with an equivalent mass of 3×10^{16} g, will require gradient measurement to 2×10^{-3} EU at 120 km altitude and 0.3×10^{-3} EU at 240 km altitude. The NASA Geopotential Research Program [6] has established as a goal a gradiometer noise level of 3×10^{-4} EU $Hz^{-1/2}$ (the accuracy of the measurement depends on the integration time available).

The instruments used to measure the gravity gradient, gradiometers, are under active development (see, e.g., [6],[11]-[13]). The technology required to achieve goals of 10^{-3} or 10^{-4} EU is formidable, but all gradiometers rest on the same fundamental principal: measuring the difference response of a pair of parallel but displaced accelerometers will give one component of W. A very simplified scheme to measure W_{zz} is shown in Fig. 2, with a somewhat more realistic version in Fig. 3. In practice one does not usually make two measurements of the acceleration and then take their difference, but measures the differential response directly, in this case as the separation of the two test masses. In some proposed gradiometers, e.g. Fig. 4, the independent test masses are replaced by a single body with a gap whose deformation is measured, but one is still effectively differencing two accelerometers.

If the gradiometer is not attached to a completely motionless platform, the measured gradient may contain errors. A linear acceleration, with no rotation, is relatively innocuous due to the phenomenon of "common mode rejection": the two test masses will be subject to the same

non-gravitational acceleration, so the difference, the measured gradient, will not be affected. Rotation of the instrument, however, will innately alter the sensed gradient as shown by (4). If the rotation has angular velocity $\omega(t)$, ignoring for simplicity the vector nature, then the T^2 term of (4) will have magnitude approximately ω^2. Measurements at the goal level of 3×10^{-4} EU $= 3 \times 10^{-13}$ sec^{-2} will be degraded if $\omega \geq 5.5 \times 10^{-7}$ $sec^{-1} = 0.1$ deg/hr. Stability at this level should be readily achievable, and if not, such rotational velocities can be easily measured and their effect removed via (4). The rotational acceleration term, $\dot{T}$, however, will interfere with measurements if $\dot{\omega} \geq 3 \times 10^{-13}$ sec^{-2}; to subtract the effects would require, over a one second integration, knowledge of ω to about 3×10^{-13} $sec^{-1} = 6 \times 10^{-8}$ deg/hr, well beyond current technology. If eight of the nine components of W are measured, the rotational acceleration effects can be removed by their anti-symmetry. However, even a very small $\dot{\omega}$ will generate large spurious gradients, and an enormous dynamic range requirement, so it will still be very important to isolate the gradiometer from rotational acceleration. Alternately, one can measure the diagonal terms only, which are not affected by the rotational acceleration; but then one must be careful to avoid contamination by the cross terms.

III. TETHERED SATELLITE SYSTEM GRADIOMETRY

The Tethered Satellite System (TSS) is a concept in which two orbiting objects (typically a large deployer such as the Space Shuttle and a smaller "subsatellite") are connected by a substantial length of cable (typically 20 to 100 km of 2 or 3 mm diameter Kevlar). The objects, seeking to travel in different orbits, pull the tether taut; the two stable configurations

are with the subsatellite directly above or below the deployer, with slight corrections for differential air drag or other forces (see Fig. 5). We are interested here in a case with a deployer in orbit above the atmosphere at, say, 220 km, and a subsatellite instrument platform deployed downward to a 120 km altitude. A free flying satellite could not stay in such a low orbit, but with the substantial mass of the deployer above the effects of drag the system can operate for many orbits, allowing continuous observation in an otherwise inaccessible region. (There does not appear to be any readily available review of the TSS; [14] provides some general discussion, and [15] is one recent paper in the open literature.)

The advantages of making gravity gradient measurements at a low altitude from a tethered subsatellite, as opposed to a free satellite in a higher orbit, are readily apparent. As discussed in Section II.B, the strength of the gravity gradient due to an anomaly decreases strongly (inverse cube) with the altitude. Also, the width of the gradient response due to a point source is proportional to altitude; at a lower altitude the signal due to distinct features will be sharper and less confused by the signals from nearby features. The more rapidly varying signal seen by a moving satellite at low altitude will require a faster response from the gradiometer (equivalent to a higher overall precision), but an error analysis performed by Kahn [16] confirms that the overall balance is in favor of the lower altitude: comparing altitudes from 80 to 160 km, the error in detecting features at a resolution of 55 km improves by up to a factor of 5 at the lower altitude using the same gradiometer at all altitudes.

Unfortunately, the subsatellite provides a less than ideal platform for delicate dynamical instruments such as gradiometers. The environment will be dynamically "noisy", being shaken and rotated with significant amplitude. The system itself has many modes of vibration, which will be excited by such internal forces as deployment, attitude and tether control, and motion of crew aboard the deployer. Additionally, there will be external forces, primarily atmospheric density variations, which will directly perturb the subsatellite and also excite the system modes. For a TSS gradiometer mission to be successful, methods must be devised to damp the vibrations, to isolate the instruments from the remaining subsatellite motions and/or to remove the effects in data processing.

For these design purposes, detailed knowledge of TSS dynamics and the perturbations to be expected is required. At SAO we are currently engaged in estimating these effects; we summarize our findings here, and indicate some plans for future research in the next section. Some of this material is presented in more detail in [17] and [18].

When discussing the dynamical noise of the TSS, we must distinguish between three interacting phenomena:

- the natural modes of vibration of the system and the associated frequencies;
- the excitation of these modes by causes external or internal, discrete or seemingly random;
- the direct perturbations of the subsatellite by external forces, the primary one of which is air drag fluctuations.

The natural modes of the system include

- tether vibration modes, both latitudinal and longitudinal ("stretching")
- the "mass-spring" mode, oscillation of the system as a whole, as if two masses on the end of a massless spring
- deployment boom oscillations
- subsatellite and orbiter attitude oscillations.

The modal frequencies have been estimated using simple models: for the tether modes, the end masses are assumed fixed; for the spring-mass mode, the tether is assumed massless; interactions between the modes are ignored. The results are listed in Table I. The excitation amplitudes are more difficult to estimate, and at the current stage of model development are largely speculative. What estimates have been made are also summarized in Table I, but these should be viewed as very approximate and non-exhaustive.

Sources of noise, either acting directly on the subsatellite or serving to excite the natural modes, include:

Internal sources:

- tether control
- thruster activation
- venting from orbiter
- overall librational motion
- crew motion on the orbiter

External sources:

- fluctuations in air drag due to density variation

- directly on subsatellite
- on the tether

- fluctuations in tether heating due to density variations
- terminator effects
- earth albedo pressure
- solar radiation pressure
- micrometeoroid impact

Where estimates of these effects have been made, these are also included in Table I.

The primary external source of dynamic noise will be fluctuations in air drag as the subsatellite traverses irregularities in density. Unfortunately, this region of the atmosphere in one almost completely unstudied. The only significant *in situ* data at low altitudes (100-150 km) appears to come from perigee passages of satellites with elliptical orbits [19]-[21]. Apart from providing only brief samples, the constantly varying altitude confuses effects due to horizontal variation and vertical stratification. Figure 3 of [20], though, does indicate substantial variations in density, up to 20%, with distance scales of tens to hundreds of kilometers. Higher altitudes allow stable circular orbits, and data suitable for detailed analysis. The most recent analysis is that of [22] and [23] for data around 250 km altitude. They find variability at all distance scales from tens of kilometers up to global scales; of particular note is the observation of discrete waves of finite extent, e.g. a wave of 250-300 km wavelength extending for only 1500 km of a total path of 4100 km. The induced acceleration from 10% density fluctuations will be about 0.5 gal.

In addition to the idealized model calculations, we have modified a general purpose TSS modeling program, SKYHOOK [14], to allow irregularities in the atmospheric density. The results of one preliminary study, in which the subsatellite encountered a single region of enhanced density, are shown in Fig. 6. The induced accelerations of the subsatellite were decomposed into components tangent to the attached tether and orthogonal. (Subsatellite attitude dynamics are not yet in the model, so there are no results on the subsatellite rotation.) After the encounter, the tangent component shows continued variability, with amplitude comparable to the direct effect during the encounter; oscillation modes have been excited quite substantially by the essentially orthogonal force. The orthogonal component behaves much more smoothly, a observation borne out by the spectra in Fig. 6. Note that the orthogonal component spectrum is some four to five orders of magnitude below the tangent spectrum. Also note the distinct peaks in the tangent spectrum; the first peak, at about 0.09 Hz, corresponds to the spring-mass mode, and the remaining eight to the eight low order longitudinal tether oscillation modes. (Higher modes are not observed due to a modeling artifact: SKYHOOK uses a lumped mass approach, dividing the tether into finite segments and approximating them by masses and springs.) The mimicking of these peaks by the orthogonal spectrum is due to the change in air density, hence orthogonal acceleration, as the subsatellite moves up and down in response to the tangent oscillations. The distinct peak at 0.001 Hz, however, is probably due to the first mode of latitudinal tether vibration.

IV. FUTURE DIRECTIONS: MODELING AND EXPERIMENT

Much work remains to properly assess the feasibility of using the TSS as a platform for gravity gradiometry. Some directions are outlined here:

A. Model Improvements

The Skyhook model program must be extended to include a number of details, including:

- attitude dynamics of the subsatellite and orbiter,
- aerodynamics of the subsatellite, including instrument and stabilization booms,
- improved atmospheric density fluctuations, e.g. a random fluctuation or a damped wave as in [23],
- dynamics of the deployment system, particularly the boom which has a transverse vibration mode with period about 2 seconds,
- gradiometer suspension and damping mechanisms.

Vibrations of the TSS with periods down to 1 second or even lower are of interest for the gradiometric measurement, and also because in this frequency region there may be complex interaction between, for instance, deployment boom vibration modes and tether oscillation modes. For Skyhook to model accurately tether longitudinal modes to period 1 second will require some sixty tether segments in the discretization. The computational cost increases rapidly with the number of segments, with a practical limit of about twenty for all but the most simple situations.

Thus, for detailed modeling we shall have to adopt a less direct approach. One possibility is to linearize the equations about a reference configuration or history and use this linearized model to simulate small departures similarly to SKYHOOK. Another direction would be to abandon direct simulation and apply methods such as random vibration analysis [24] to proceed directly from a statistical description of the system perturbations (such as drag variations) to a statistical description of the responses of interest. This method would also rely on a linearized model of the TSS, but we would not actually evolve the model in time. Probably both of these approaches will be advantageous for studying different circumstances; e.g., it is hard to see how the statistical method would cope with an impulsive disturbance such as a thruster.

B. TSS Demonstration Missions

NASA and PSN/CNR (the Italian spacae agency) have announced [25] the flight of at least one, and tentatively three, demonstration missions of the TSS for the purpose of studying the system and utilizing it for scientific experiments. The first mission is to be an electrodynamic tether, a 20 km conductor deployed upward from the orbiter and intended largely to examine interactions with the plasma. The second (tentative) mission would be atmospheric, with a 100 km tether deployed downward to an altitude of 120-150 km, and the third would be another electrodynamic mission.

Included in the subsatellite core equipment to be provided by NASA and PSN/CNR are a three axis linear accelerometer and a three axis rate integrating gyro. These instruments will allow the measurement of the dynamic characteristics of the system and (on the second mission) direct

observation of the perturbations induced by atmospheric drag fluctuations. SAO [18] and others have submitted proposals to analyze the data from the accelerometers and gyros.

The observations will be useful directly in providing a picture of the dynamic environment in an actual deployed system. In particular, the effects of atmospheric drag irregularities should be observable by rotating the accelerometer data to a system tangent and orthogonal to the tether. From the spectra in Fig. 6 it is seen that the direct effect of the drag variations is far stronger than the residual response in the orthogonal direction; and it will probably prove possible to utilize the strong spectral signature of the tangent component to perform the rotation. This is likely to be the first solid data on density variations in the lower thermosphere, and thus crucial in the design of the gradiometer mission.

Simply observing the dynamic noise will not be adequate. The gradiometer mission will almost certainly require damping mechanisms or carefully designed instrument suspension, specifically to alter the noise. The dampers, suspension and the gradiometer itself will become part of the system, quite possibly affecting its overall behavior; the noise environment cannot simply be taken as a given. Thus, a major contribution of the demonstration missions will be the validification and refinement of detailed models of the TSS. The modifications required for the gradiometric mission can then be confidently modeled. Of particular interest will be the presence of known system perturbations, such as thruster firings and reel control. These will allow detailed comparison of model predictions with observed response.

Detailed objectives for each flight are:

Mission I (upward deployed, electrodynamic tether):

- measure system responses and natural frequencies
- compare with theory and simulations
- obtain estimates of system damping
- utilize known perturbations due to thrusters

Mission II (downward deployed, atmospheric mission):

- observe effects of atmospheric density fluctuations
- measure properties of this different system:
  - different tether material
  - possibility of resonance between subsatellite attitude oscillations and longitudinal tether oscillations
- fly a simple, non-cryogenic gradiometer (see Section C below)

Mission III (upward):

- repeat and refine analyses of Mission I
- possibly test noise damping methods

C. A Non-Cryogenic Gradiometer for the Second Demonstration Mission

Observations of the dynamic noise environment will certainly be useful in designing a dedicated gradiometric mission. But one would also like to directly measure the gradiometric noise with a gradiometer, rather than rely solely on extrapolation from the accelerometer and gyro data. The

second proposed demonstration mission is the most suitable of the three for mounting a gradiometer: one will have had the opportunity to observe system dynamics on the first mission and possibly implement some form of damping mechanism; and the system itself and the atmospheric perturbations will provide the closest similarity to the dedicated mission.

The subsatellite for the demonstration flights imposes some significant constraints on the size and mass allowable for an instrument. Most of the instruments under development for an eventual gradiometric mission (either free flying or on the TSS) require cryogenic cooling and are thus too large to compete with other experiments and system equipment for space in the 1.5 meter diameter subsatellite. However, IFSI-CNR in Frascati, Italy has under development a non-cryogenic gradiometer [12] with a sensitivity of about 3×10^{-2} EU $Hz^{-1/2}$. This is two orders of magnitude less sensitive than the eventual design goal, but should provide adequate information on the dynamic environment and may produce data of geodynamic interest if dampers are implemented for the second mission. This gradiometer, in addition to being non-cryogenic, also employs very small proof masses, 0.5 kg each (two being required); it consists of a pair of sensitive accelerometers with torsional deflection of the proof mass.

Testing of sensitive gradiometers on the Earth's surface is difficult, due to the extreme isolation from vibration which must be achieved while still maintaining mobility relative to a large test mass. SAO is developing a testing technique [11] in which a gradiometer falls freely down an evacuated tube. A ring around the tube forms the gradient generating test mass and the gradiometer falls through this localized area of enhanced gradient. By suitably choosing the height of the tube and the size of the mass ring we can adjust the temporal width and magnitude of

the measured pulse. The proposed tower is 11 meters tall with 1 m diameter; the ring mass is 9 kg.

V. SUMMARY

The use of gravity gradiometry to measure the Earth's gravity field is probably the next step after the upcoming Geopotential Research Mission. Flying a gradiometer in a tethered subsatellite at low altitude, as opposed to a freely orbiting satellite, has the dual benefits of increasing gradient signal levels due to mass distribution near the Earth surface and narrowing the pulse width due to a localized anomaly; this could either improve the accuracy achievable or reduce the accuracy demanded of the gradiometer. However, the subsatellite is expected to be a dynamically noisy environment due to the influence of atmospheric density irregularities encountered and to interaction with the rest of the system. Characterizing this environment and evaluating the feasibility of dynamic noise abatement methods is a topic of current research. Accelerometers and gyros on the demonstration flights of the Tethered Satellite System will provide an opportunity to measure the dynamic environment and test system models, in preparation for final evaluation and design of a dedicated mission.

REFERENCES

[1] W. M. Kaula, An Introduction to Planetary Physics: The Terrestrial Planets. New York: John Wiley & Sons, 1968, Section 2.1.

[2] J. C. Harrison, "Gravity, Earth's," in R. G. Lerner and G. L. Trigg, eds., Encyclopedia of Physics. Reading, MA: Addison-Wesley, 1981, pp. 369-371.

[3] K. Lambeck, "The gravitational mechanics of the Earth," in D. G. Smith, ed., The Cambridge Encyclopedia of Earth Sciences. New York: Crown/Cambridge, 1981, pp. 93-108.

[4] F. S. Grant and G. F. West, Interpretation Theory in Applied Geophysics. New York: McGraw-Hill, 1965.

[5] W. A. Heiskanen and H. Moritz, Physical Geodesy. San Francisco: W.H. Freeman, 1967.

[6] W. C. Wells, ed., Spaceborne Gravity Gradiometers, Proceedings of a workshop held at NASA Goddard Space Flight Center, Greenbelt, Maryland, February 28-March 2, 1983. NASA Conference Publication 2305, 1984.

[7] T. Keating, "Geopotential Research Mission (GRM)," J. Astronautical Sci., vol. 32, pp. 145-158, 1984.

[8] E. M. Gaposchkin, "Geopotential Mapping Using Satellite to Satellite Tracking Data," Paper GD41-06, EOS, vol. 65, p. 196, 1984.

[9] W. T. Dewhurst, "The Observation of Vertical Gravity Gradients: Operational Consideration and Survey Results," Paper G12-02, EOS, vol. 65, p. 180, 1984.

[10] C. C. Goad and M. M. Chin, "The contribution of Vertical Gravity Gradients and Geoid Height Differences to Geoid Modeling," Paper G12-09, EOS, vol. 65, p. 181, 1984.

[11] F. Fuligni and M. D. Grossi, Research Relative to the Development of a Cryogenic Microwave Cavity Gradiometer for Orbital Use, Semiannual Report No. 2, NASA Grant NAG5-338, July 1984.

[12] F. Fuligni and M. D. Grossi, High Sensitivity Geometric Displacement Sensors for the Measurement of Weak Forces and Torques, Final Report, NASA-IRP Grant 671-7056, August 1984.

[13] H. J. Paik, H. A. Chan, M. V. Moody and J. W. Parke, "Three-Axis Superconducting Gravity Gradiometer for Spaceborne Gravity Survey," Paper GD41-09, EOS, vol. 65, p. 196, 1984.

[14] P. M. Kalaghan, D. A. Arnold, G. Colombo, M. D. Grossi, L. R. Kirschner, and O. Orringer, Study of the Dynamics of a Tethered Satellite System (SKYHOOK), Final Report, NASA Contract NAS8-32199, March 1978.

[15] A. K. Banerjee and T. R. Kane, "Tether Deployment Dynamics," J. Astronautical Sci., vol. 30, pp. 347-365, 1982.

[16] W. Kahn, private communication, 1983.

[17] G. E. Gullahorn, M. D. Grossi and E. Lorenzini, Investigation of Dynamic Noise Affecting Geodynamics Information in a Tethered Subsatellite, Final Report, NASA Grant NAG5-325, May 1984.

[18] G. E. Gullahorn, Investigation and Measurement of Dynamic Noise in Tethered Satellite Systems, Proposal P1437-7-84 submitted in response to NASA AO No. OSSA-1-84, July 1984.

[19] F. A. Marcos and K. S. W. Champion, "Gravity Waves Observed in High Latitude Neutral Density Profiles," Space Research XII, pp.791-796, 1972.

[20] C. A. Reber, A. E. Hedin, D. T. Pelz, W. E. Potter and L. H. Brace, "Phase and Amplitude Relationships of Wave Structure Observed in the Lower Thermosphere," J. Geophys. Res., vol. 80, pp. 4576-4580, 1975.

[21] W. E. Potter, D. C. Kayser, and K. Mauersberger, "Direct Measurement of Neutral Wave Characteristics in the Thermosphere," J. Geophys. Res., vol. 81, pp. 5002-5012, 1976.

[22] S. H. Gross, C. A. Reber and F. T. Huang, "Large-Scale Waves in the Thermosphere observed by the AE-C Satellite," IEEE Trans. Geosci. Remote Sensing, vol. GE-22, pp. 340-352,1984.

[23] S. H. Gross and F. T. Huang, "Medium Scale Gravity Waves in the Thermosphere Observed by the AE-C Satellite," preprint, 1984.

[24] N. C. Nigam, Introduction to Random Vibrations. Cambridge, MA: MIT Press, 1983.

[25] National Aeronautics and Space Administration and Piano Spaziale Nazionale, Announcement of Opportunity for Tethered Satellite System, AO No. OSSA-1-84, April 15 1984.

TABLE I

Sources and Modes of Dynamic Noise (0.001 Hz. - 1 Hz.)

Case A: 100 km tether, upward, Orbiter at 230 km, 28 degree inclination.
Case B: 20 km tether, downward, Orbiter at 295 km, 28 degree inclination.

EFFECT	SPECTRUM (Hz)	TYPICAL MAGNITUDES LINEAR ACCELERATION (gal)	ROTATION RATE (rad/sec)	ASSUMPTIONS/COMMENTS
Spring-Mass Mode	A: 0.01	2	TBD	Residual from deployment.
	B: 0.03	TBD	TBD	
Longitudinal Tether Oscillations	A: 0.03 n	.001-.005	TBD	n = 1,2,3,... Excited by subsatellite attitude osc.
	B: 0.2 n	TBD	TBD	n = 1,2,3,...
Latitudinal Tether Oscillations	A: 0.001 n	TBD	TBD	n = 1,2,3,...
	B: 0.002 n	TBD	TBD	n = 1,2,3,...
Deployment Boom Vibrations	0.5	TBD	TBD	First normal mode.
Subsatellite Attitude Dynamics				Excited by TSS librations.
In Plane	A: 0.2	1	0.022	
	B: 0.1	0.04	0.002	
Out of Plane	A: 0.2	0.04	0.001	
	B: 0.1	0.02	0.001	
Radial	A: TBD	0.02	TBD	
	B: TBD	0.0003	TBD	
Drag Fluctuation on Subsatellite	Broadband	A: 0.5	0.002	10 % density fluctuations
		B: 0.001	3 E-6	
Crew Motion in Orbiter	Transient	0.1	TBD	100 kg person, 1/2 m/sec vel.
	Broadband	0.0001-0.001	TBD	small motions, writing, etc.

FIGURE CAPTIONS

Fig. 1. Gravity gradient due to a point mass. The shape functions of Equ. (7) in the text are plotted as a function of distance along a straight horizontal path for three paths, one directly over the mass and two whose closest horizontal approaches are one and three times the altitude. The gradient is scaled by the factor (GM/Z^3) and the along path coordinate by Z, where Z is the altitude. Note that the gradient response is both weaker and more extended as the path offset increases.

Fig. 2. A schematic gradiometer for measuring the single component W_{zz}. In order that both masses will have the same displacement for the same gravitational acceleration, $k_1/m_1 = k_2/m_2$. Each mass/spring combination responds to the vertical (z) component of the gravity vector, and since they are at different heights, any vertical gradient in this component will appear as a differential response. The observed quantity is the vertical separation ΔZ.

Fig. 3. Cross section of a gradiometer realizing the principle of Fig. 2 in somewhat greater engineering detail. The springs are tubular.

Fig. 4. A gradiometer which measures the distortion of a slot in a plate, forming the equivalent of two separated test masses. The configuration shown measures the gradient in several directions allowing reconstruction of the gradient tensor; however, the six measurements will not allow full reconstruction in the presence of an antisymmetric part caused by rotation (see Equ. 4).

Fig. 5. A schematic illustration of the Tethered Satellite System (TSS).

Fig. 6. Results of a simulation in which the subsatellite encountered an atmospheric density enhancement of 20% extending for 100 km. The residual accelerations of the subsatellite after the encounter are plotted (a) for the component tangent to the tether and (b) orthogonal to the tether in the orbit plane. The tangent accelerations are comparable to the direct acceleration produced (0.082 gal in approximately the orthogonal direction) by the encounter, and are complex in form. The orthogonal accelerations are much smaller in magnitude, and smoother. The two time series in (a) and (b) were Fourier analyzed and the magnitudes of the resulting spectra are shown in (c). The orthogonal component is weaker and strongly dominated by the first two modes. See the text for discussion of the modes.

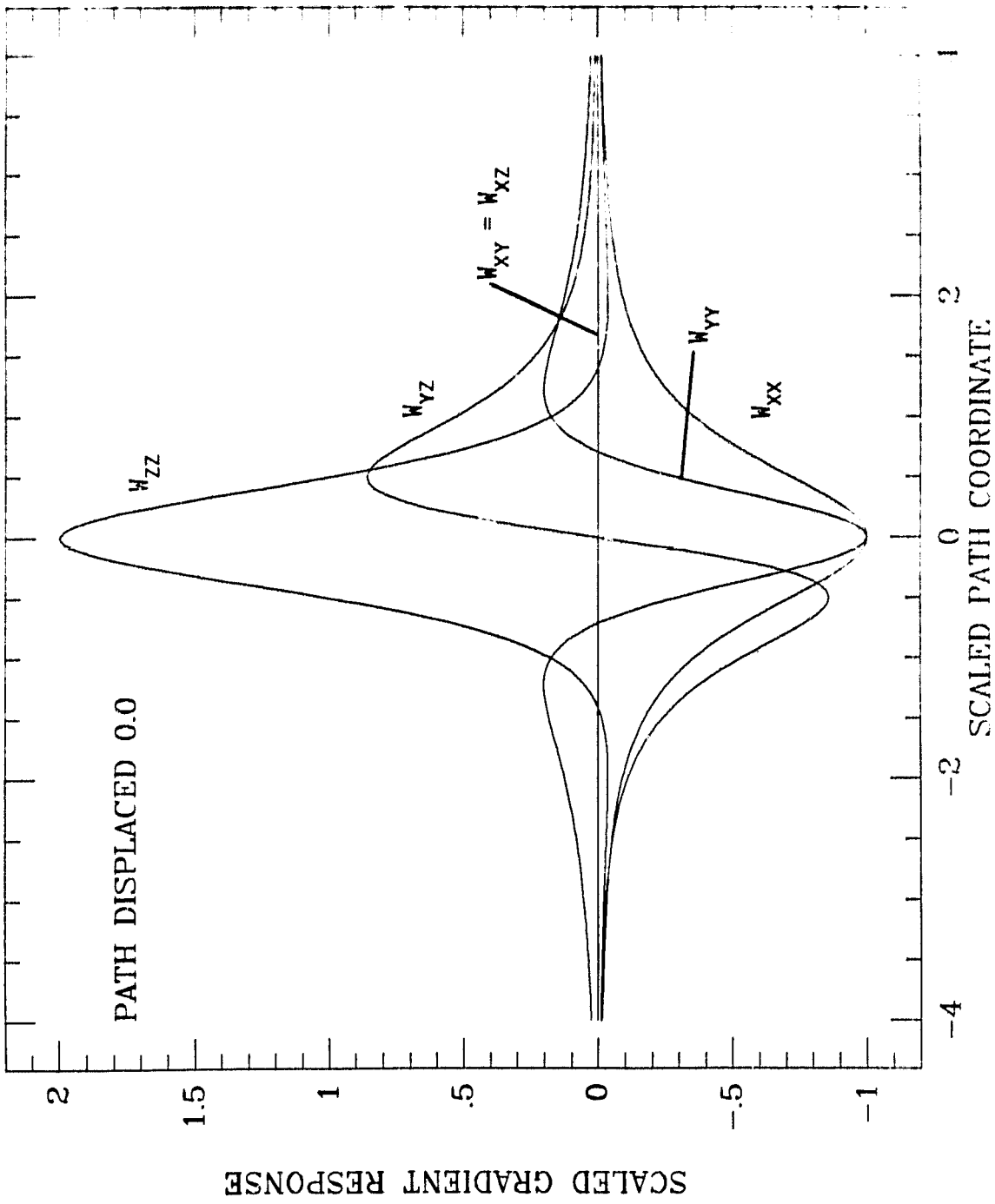
PATH DISPLACED 0.0
W_{ZZ}
W_{YZ}
$W_{XY} = W_{XZ}$
W_{YY}
W_{XX}
2
1.5
1
.5
0
-.5
-1
-4
-2
0
2
SCALED PATH COORDINATE
SCALED GRADIENT RESPONSE

Fig. 1

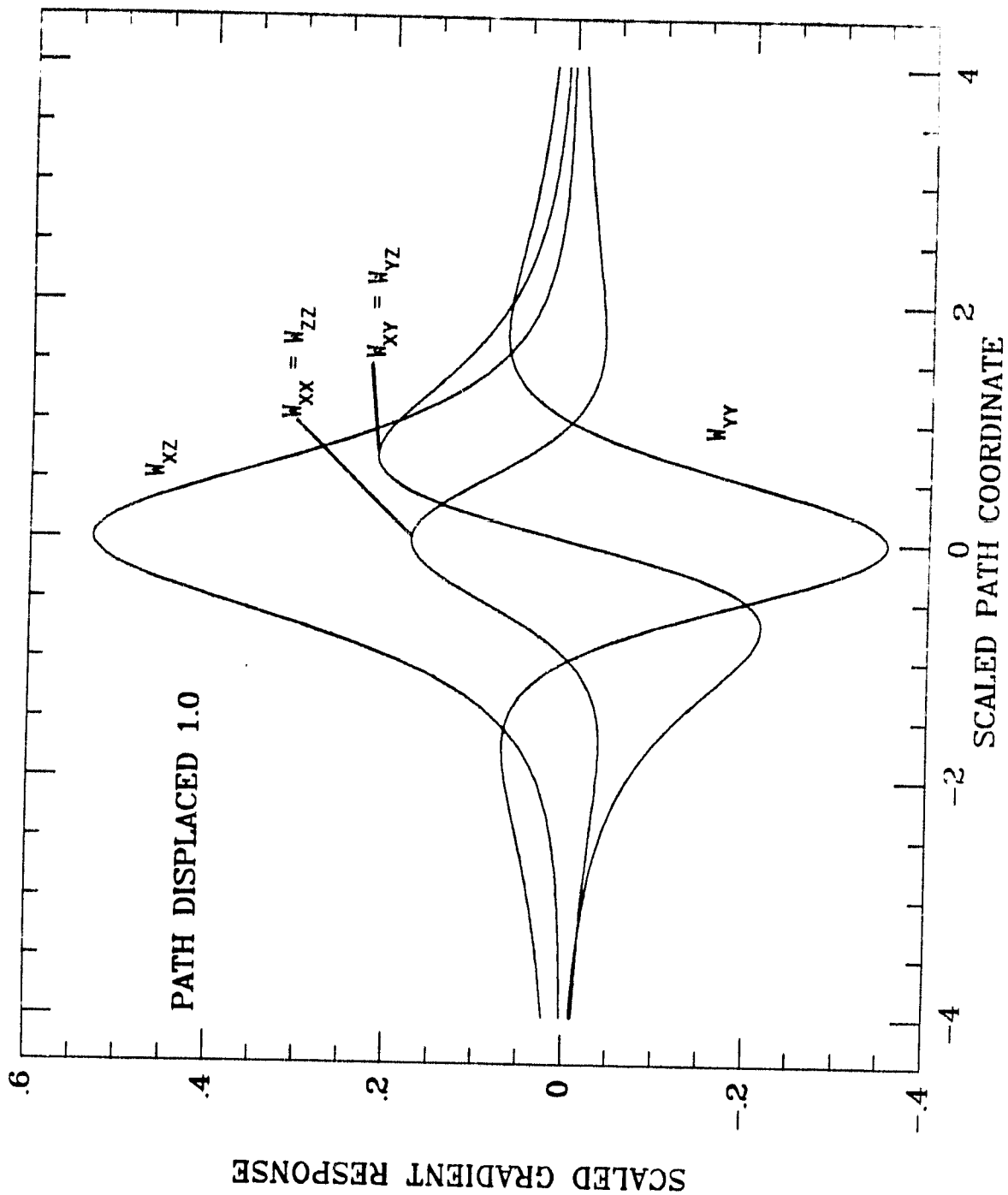

Fig. 1 (continued)

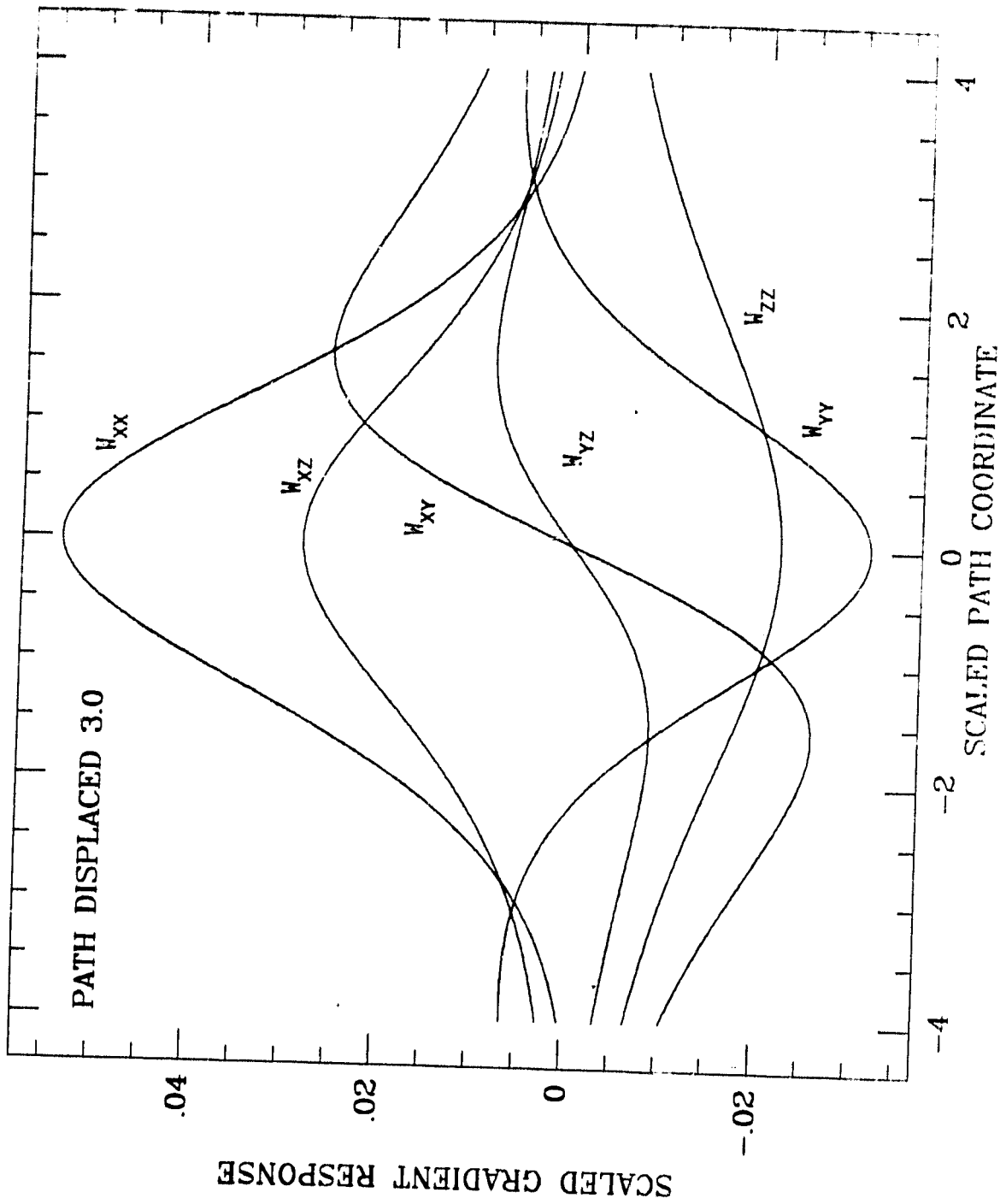

Fig. 1 (continued)

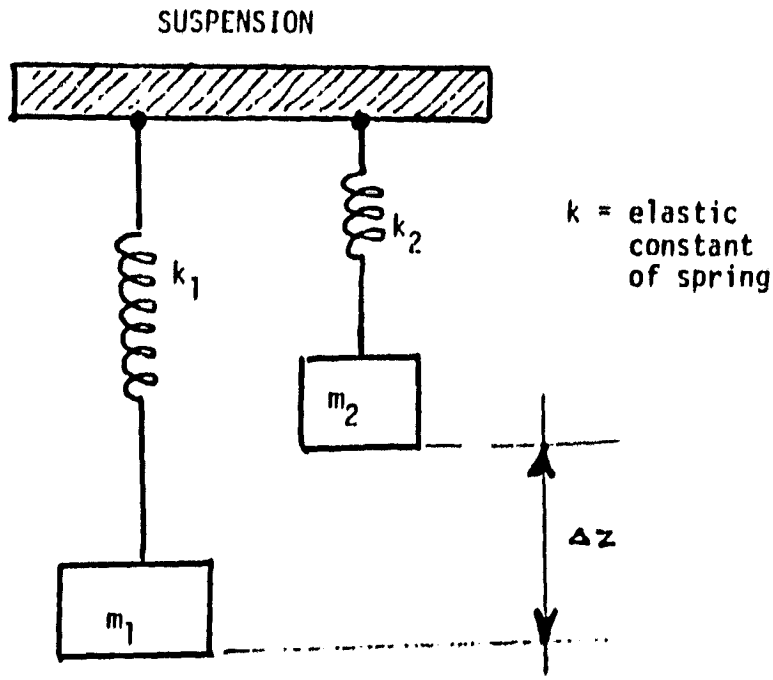

Fig. 2

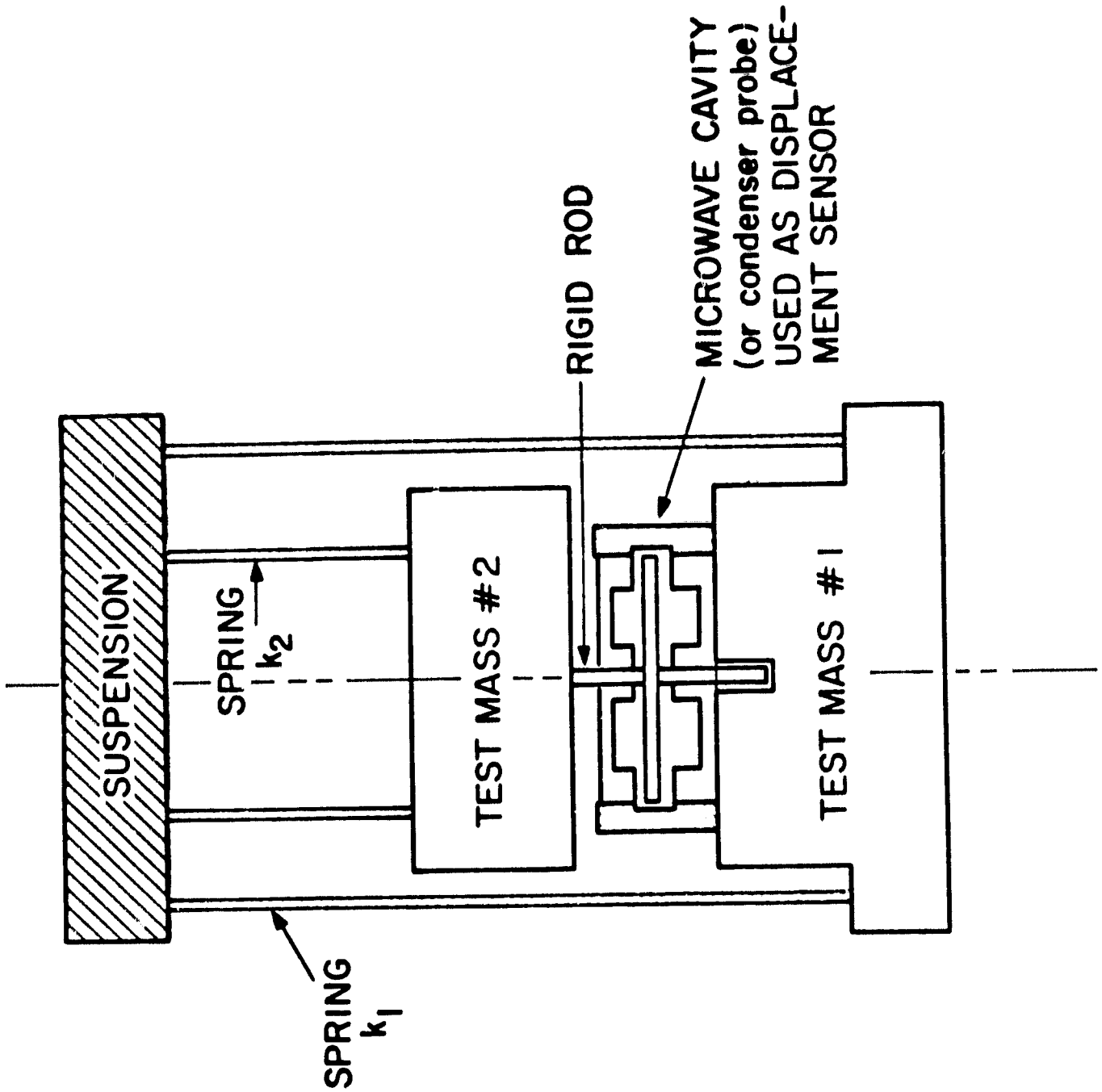
SUSPENSION
SPRING
k_2
TEST MASS #2
RIGID ROD
MICROWAVE CAVITY
(or condenser probe)
USED AS DISPLACE-
MENT SENSOR
TEST MASS #1
SPRING
k_1

Fig. 3

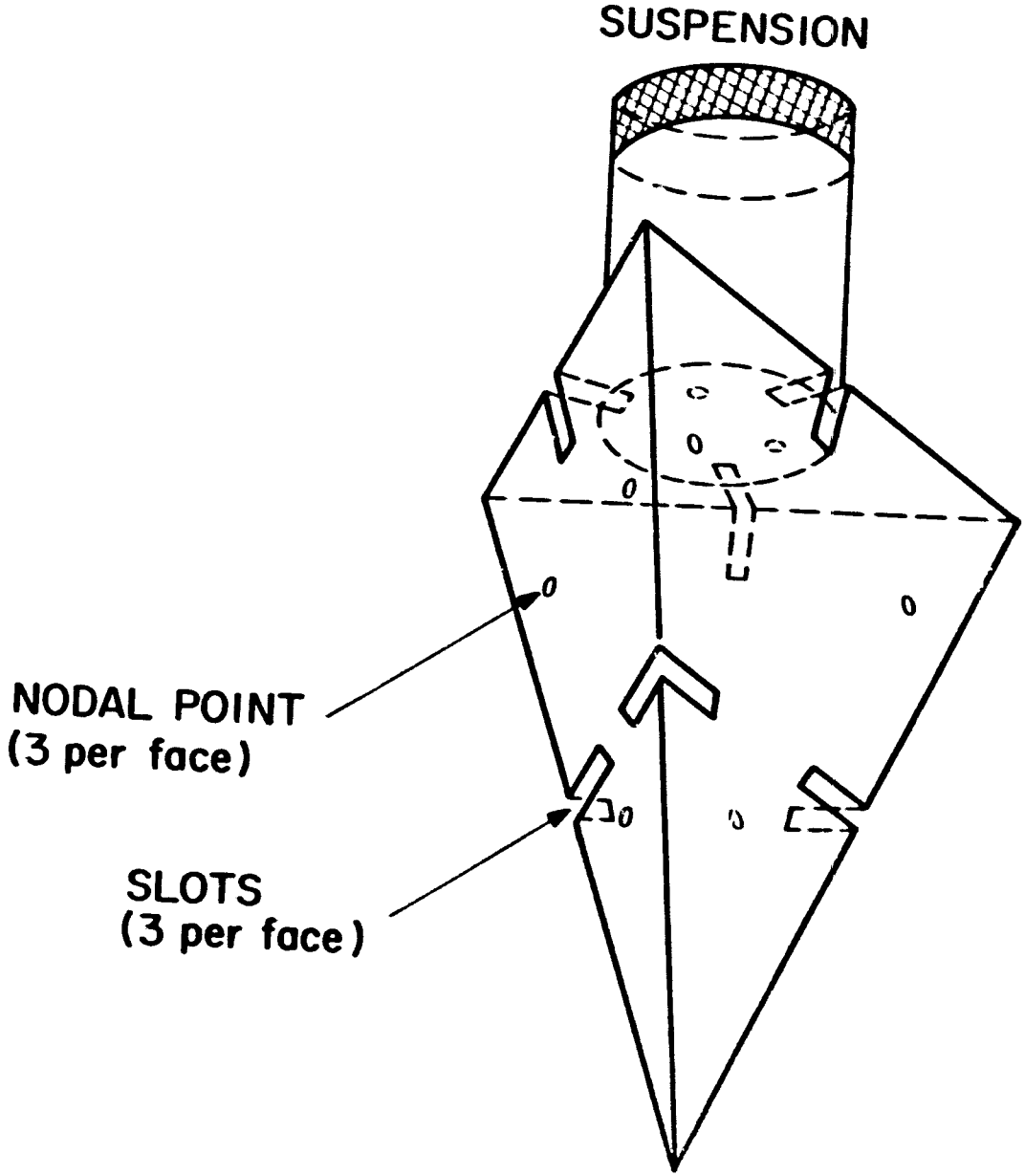

Fig. 4

408-090

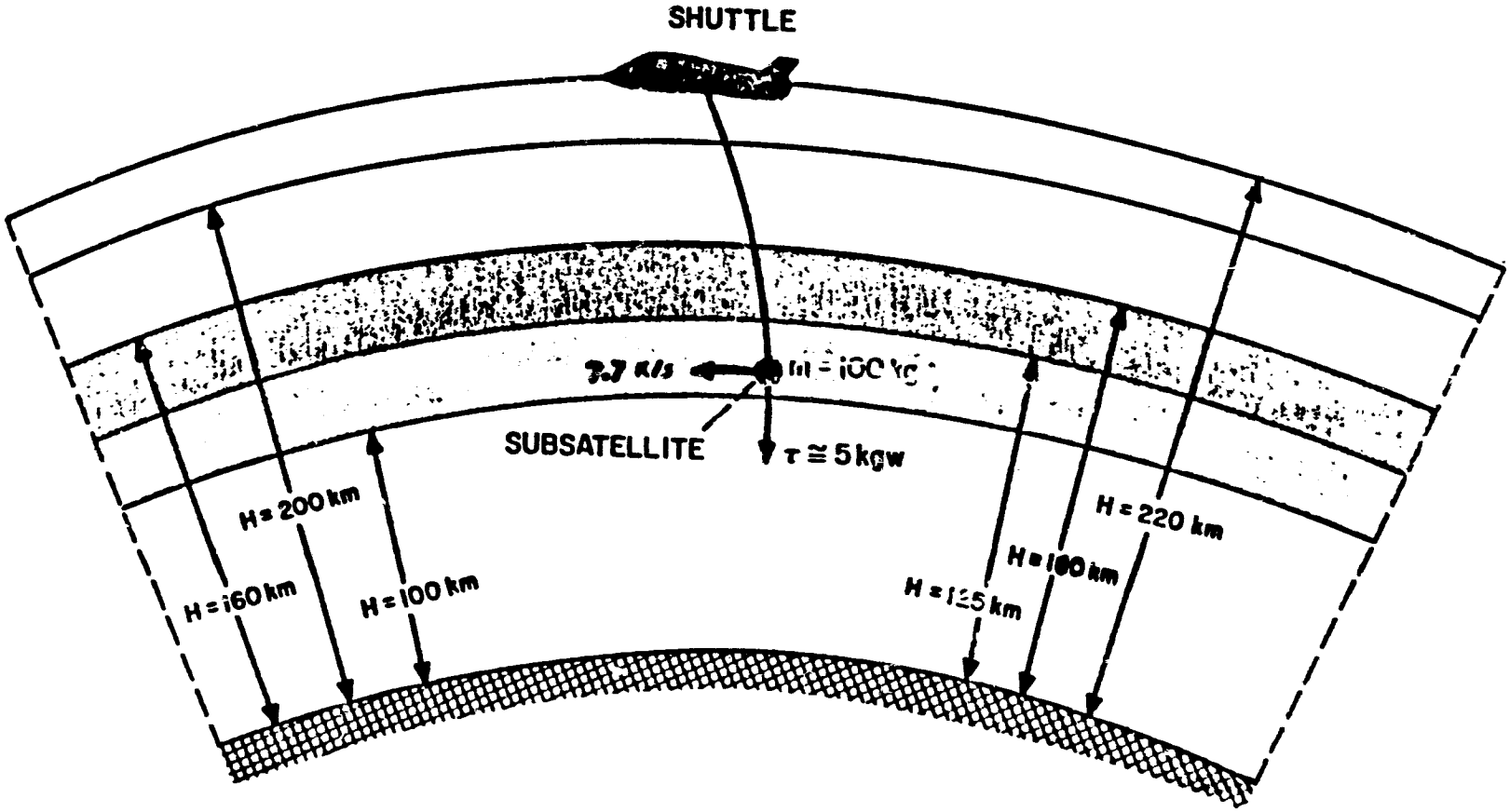

Fig. 5

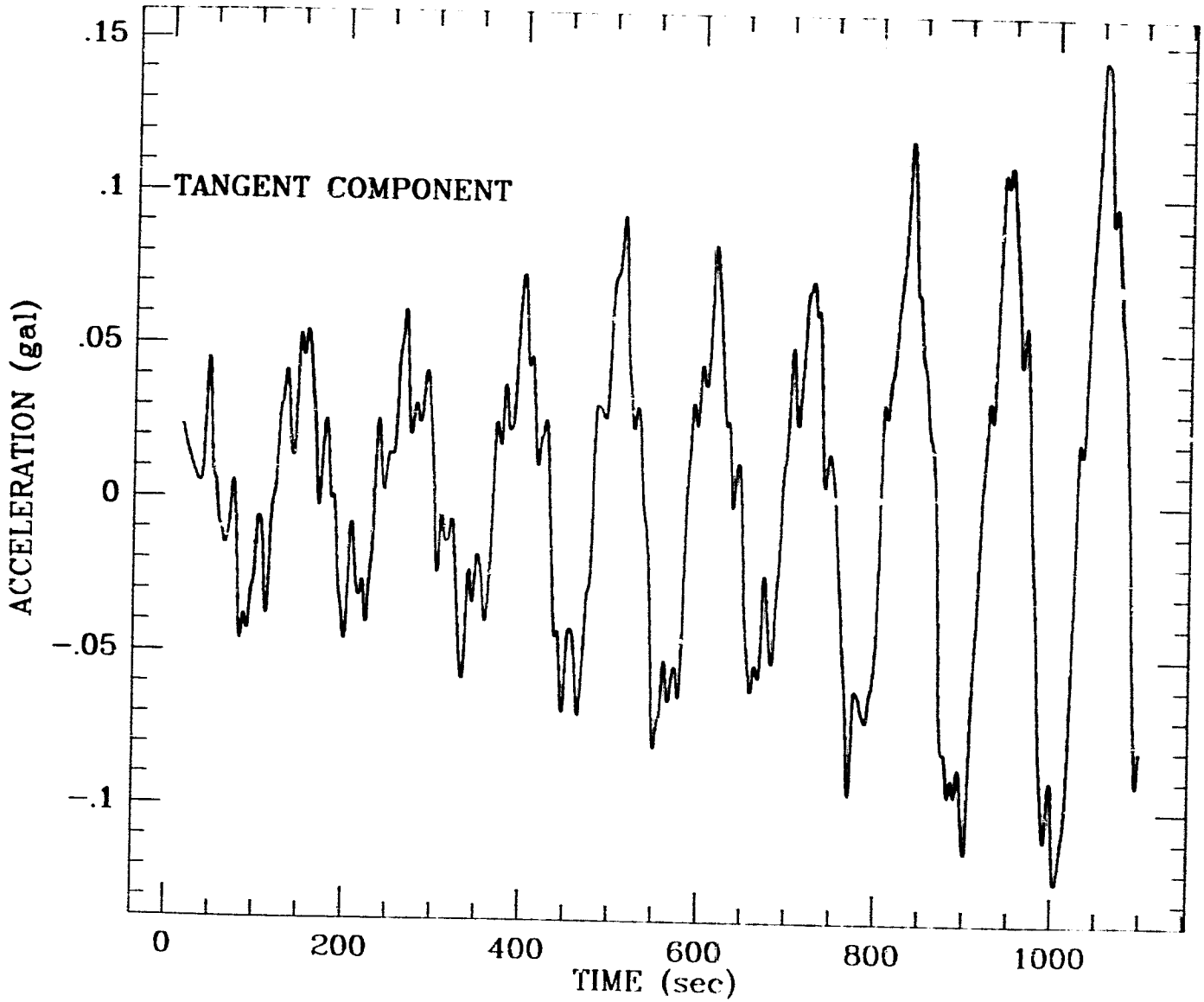
.15
.1
.05
0
−.05
−.1
TANGENT COMPONENT
ACCELERATION (gal)
0
200
400
600
800
1000
TIME (sec)

Fig. 6a

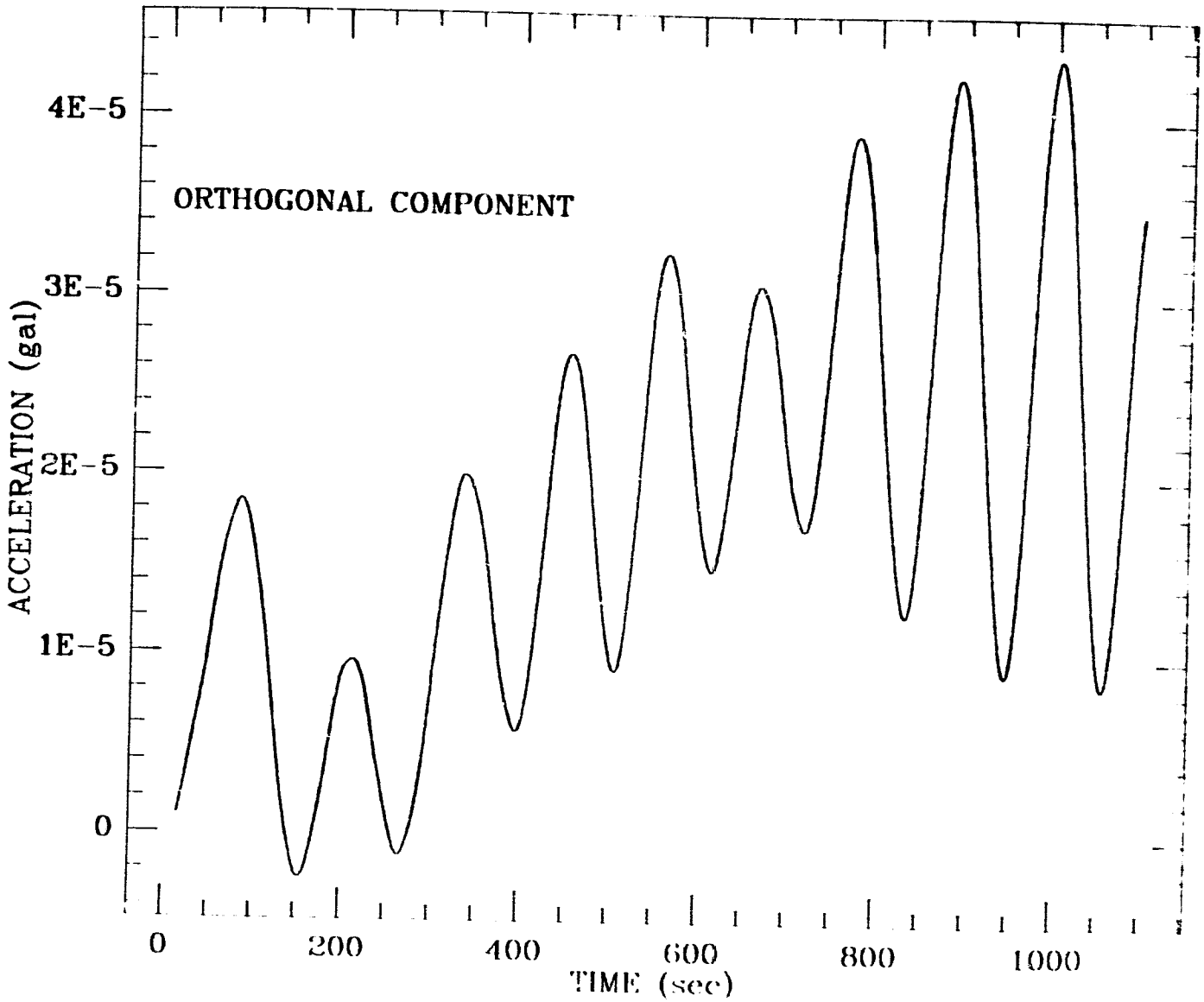
ORTHOGONAL COMPONENT
ACCELERATION (gal)
4E-5
3E-5
2E-5
1E-5
0
0
200
400
600
800
1000
TIME (sec)

Fig. 6b

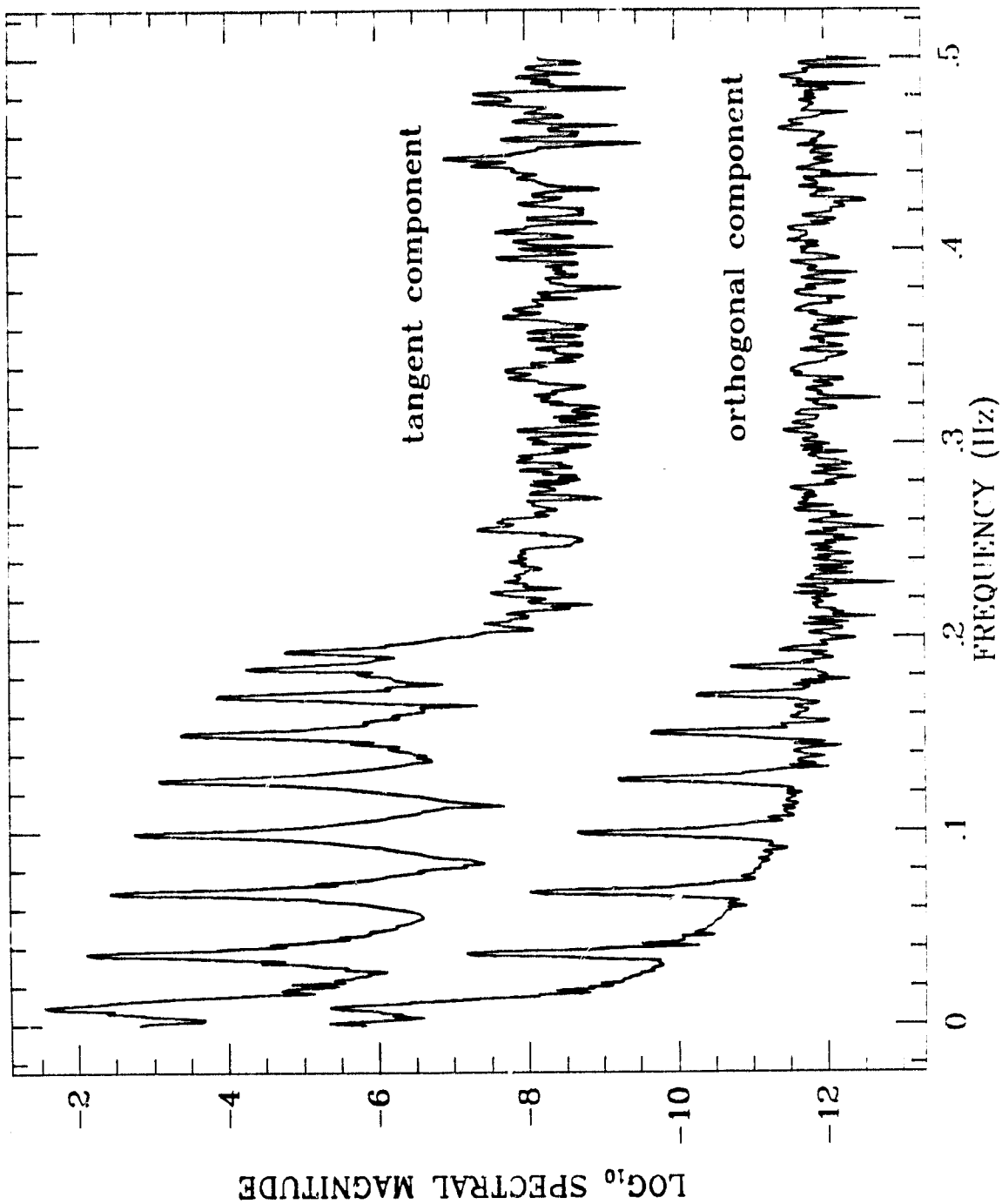
tangent component
orthogonal component
LOG10 SPECTRAL MAGNITUDE
-2
-4
-6
-8
-10
-12
0
.1
.2
.3
.4
.5
FREQUENCY (Hz)

Fig. 6c